

An assessment of equatorial Atlantic interannual variability in OMIP simulations

Arthur Prigent¹ and Riccardo Farneti¹

¹Earth System Physics, The Abdus Salam International Centre for Theoretical Physics (ICTP), Trieste, 34134, Italy

Correspondence: Arthur Prigent (aprigent@ictp.it)

Abstract. The eastern equatorial Atlantic (EEA) seasonal cycle and interannual variability strongly influence the climate of the surrounding continents. It is thus crucial that models used in both climate predictions and future climate projections are able to simulate them accurately. In that context, the EEA ~~seasonal cycle~~ monthly climatology and interannual variability are evaluated over the period 1985-2004 in models participating to the Ocean Model Intercomparison Project Phases 1 and 2 (OMIP1 and 5 OMIP2). The main difference between OMIP1 and OMIP2 simulations is their atmospheric forcing: CORE-II and JRA55-do, respectively. ~~Seasonal cycles~~ Monthly climatologies of the equatorial Atlantic zonal ~~winds~~ wind, sea level anomaly and sea surface temperature in OMIP1 and OMIP2 are comparable to reanalysis ~~datasets~~ products. Yet, some discrepancies exist in both OMIP ensembles: the thermocline is too diffusive and there is a lack of cooling during the development of the Atlantic cold tongue. ~~In addition, the vertical ocean velocity in the eastern equatorial Atlantic in boreal summer is larger in OMIP1 than in OMIP2 simulations.~~ The EEA interannual sea surface temperature variability during May-June-July in the OMIP1 ensemble mean is found to be 51% larger (0.62 ± 0.04 °C) than the OMIP2 ensemble mean (0.41 ± 0.03 °C). Likewise, the May-June-July interannual sea surface height variability in the EEA is 33% larger in the OMIP1 ensemble mean (0.02 ± 0.002 m) than in the OMIP2 ensemble mean (0.015 ± 0.002 m). Sensitivity experiments demonstrate that the discrepancy in interannual sea surface temperature ~~variability and sea surface height variabilities~~ between OMIP1 and OMIP2 is mainly 15 ~~attributed~~ attributable to their wind forcing, and specifically to its variability. While the April-May-June zonal wind variability in the western equatorial Atlantic is similar in both forcing, the zonal wind variability peaks in April for JRA55-do and in May for CORE-II. ~~Differences in surface heat fluxes between the atmospheric forcing datasets have no significant impacts on the simulated interannual SST variability.~~

1 Introduction

20 ~~Various regions of the globe are marked with large~~ The sea surface temperature (SST) ~~variability (defined as the standard deviation of the monthly mean SST anomalies, Figure ??).~~ In the extratropical regions, high SST variability (exceeding 1.2 °C) is observed in areas with strong SST gradients such as the Gulf Stream and Malvinas Current in the Atlantic Ocean, the Agulhas Current in the Indian Ocean, and the Kuroshio Current in the Pacific Ocean (Deser et al. (2009), Figure ??a). Within the tropics, high SST variability occurs at the interannual timescale in the equatorial Pacific, mainly driven by El 25 Niño/Southern Oscillation (ENSO), and in the equatorial Atlantic, driven by the Atlantic zonal and meridional modes. The

simulation of SST variability by state-of-the-art ocean general circulation models (OGCMs) participating to the Ocean model intercomparison Project (OMIP) Phases 1 and 2 are shown in Figures ??b and e, respectively. In comparison to the OMIP1 ensemble (Figure ??b), the OMIP2 ensemble mean (Figure ??c) depicts higher SST variability in eddy-rich regions like the Gulf Stream, Kuroshio, Malvinas and Agulhas current as well as in eastern boundary upwelling systems, most notably in the Angola-Benguela Area and off the coasts of Peru and Dakar (Figure ??d). Conversely, in the equatorial Pacific and Atlantic Oceans, the OMIP1 ensemble mean exhibits higher SST variability than the OMIP2 ensemble mean (Figure ??d). This study specifically addresses the discrepancies in the representation of interannual SST variability in the equatorial Atlantic between the OMIP1 and OMIP2 ensembles.

Standard deviation of SST anomalies for (a) ORA-S5, (b) the OMIP1 ensemble mean, (c) the OMIP2 ensemble mean spanning from January 1985 to December 2004. (d) Difference between the OMIP2 ensemble mean minus the OMIP1 ensemble mean. The grey, blue, and green boxes represent the NINO3.4 (170°W-120°W, 5°S-5°N), ATL3 (20°W-0°E, 3°S-3°N), and ATL4 (40°W-20°W, 3°S-3°N) regions, respectively.

The SST in the equatorial Atlantic exhibits a marked seasonal cycle closely related to the seasonal displacement of the intertropical convergence zone (ITCZ). In March-April-May (MAM), highest temperatures are observed in the equatorial region ($>27^{\circ}\text{C}$) as the sun is positioned directly overhead, resulting in maximum incident solar radiation (Xie and Carton, 2004). In this season, the ITCZ is situated close to the equator leading to weak trade winds that cause a deep thermocline in the eastern equatorial Atlantic (EEA). As the year progresses the ITCZ migrates northward, and the southeasterly winds intensify. This shift leads to a shoaling of the thermocline, enhanced upwelling and vertical mixing as well as intensified evaporation in the EEA (Lübbecke et al., 2018). Consequently, from May to June, the Atlantic cold tongue (ACT) forms east of 20°W, persisting until September with SSTs below 25 °C. The initiation of the ACT and the West African Monsoon (WAM) have been observed to be interconnected. In fact, delayed onsets of the ACT and WAM are associated with anomalously warm SSTs in the EEA (Brandt et al., 2011; Caniaux et al., 2011).

Every few years, the SST in the EEA experiences large deviations ($>1.5^{\circ}\text{C}$) from its climatology, exerting significant influence on the climate of the neighbouring continents (Hirst and Hastenrath, 1983; Folland et al., 1986; Nobre and Shukla, 1996). The EEA depicts notable interannual SST variability, particularly in boreal summer, within resulting from the Atlantic Niño or Atlantic zonal mode (Servain et al., 1982; Zebiak, 1993; Keenlyside and Latif, 2007; Lübbecke et al., 2018). Atlantic Niños (Niñas) are characterised by warm (cold) SST anomalies developing in the ATL3 region (Zebiak (1993); 20°W-0°E, 3°S-3°N, indicated by the blue box in Figure 1). The enhanced ATL3 interannual SST variability denotes two peaks, one in May-June-July (MJJ), during the development of the ACT, is the result of the Atlantic zonal mode or Atlantic Niño mode (Servain et al., 1982; Zebiak, 1993; Keenlyside and Latif, 2007; Lübbecke et al., 2018). Atlantic and driven by Atlantic Niños (Niñas) are characterised by warm (cold) SST anomalies developing in the ATL3 region (Figure 1a), and another in November-December driven by the Atlantic Niños II (Okumura and Xie, 2006). The interannual SST variability in the EEA is phased-locked to the seasonal cycle, with maximum variability occurring in boreal summer when the thermocline is shallow and the surface-subsurface coupling is maximum (Keenlyside and Latif, 2007). The underlying dynamics of the Atlantic Niño bear some resemblance to that observed during El Niño/Southern Oscillation (ENSO) in the Pacific ocean (Zebiak, 1993).

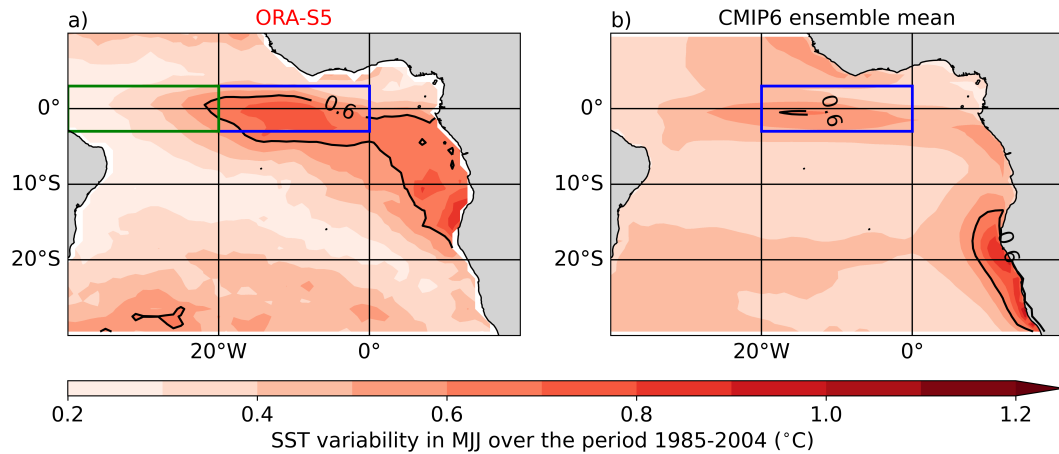


Figure 1. Interannual SST variability in the tropical Atlantic during MJJ. Standard deviation of the MJJ-averaged SST anomalies for (a) ORA-S5, (b) CMIP6 ensemble mean, (c) the OMIP1 ensemble mean, and (d) the OMIP2 ensemble mean spanning from January 1985 to December 2004. The CMIP6 ensemble is composed of 55 models listed in Supplementary Table S1. The blue and green boxes represent the ATL3 (20°W-0°E, 3°S-3°N) and ATL4 (40°W-20°W, 3°S-3°N) regions, respectively.

It involves, involving a coupling between SST, zonal wind stress and ocean heat content as described by the Bjerknes feedback (Bjerknes, 1969). The Bjerknes feedback (BF; Bjerknes, 1969). The BF can be decomposed into three components: (1BF1) the forcing of western equatorial Atlantic (ATL4; 40°W-20°W, 3°S-3°N; green box in Figure 1a) zonal wind anomalies by SST anomalies in the ATL3 region; (2BF2) the forcing of thermocline depth anomalies in the ATL3 region by zonal wind anomalies in the ATL4; (3BF3) the forcing of SST anomalies in the ATL3 by local thermocline depth anomalies. All three components of the Bjerknes feedback-BF components are active in the equatorial Atlantic although they are generally weaker and display a stronger seasonal modulation than those observed in the Pacific (Keenlyside and Latif, 2007; Lübbecke and McPhaden, 2017; Dippe et al., 2019). The study of Atlantic Niños is of particular importance as they have shown to influence the climate of the neighbouring continents (Hirst and Hastenrath, 1983; Folland et al., 2009), the El Niño/Southern Oscillation (Rodríguez-Fonseca et al., 2009), the Indian Monsoon (Kucharski et al., 2008), and European climate (Cassou et al., 2005). Atlantic Niños may also drive equatorial Atlantic interannual chlorophyll-a concentration variability (Chenillat et al., 2021).

Despite substantial warm biases found in state-of-the-art coupled general circulation models (CGCM) in the EEA (Davey et al., 2002; Richter and Tokinaga, 2020; Farneti et al., 2022), CGCMs are still capable of reproducing the Bjerknes feedback BF (Deppenmeier et al., 2016). A number of them manage to simulate realistic interannual SST variability within the ATL3 during boreal summer (Figure 1b; see also Richter and Tokinaga, 2020). However, while the CGCM ensemble mean depicts too weak interannual SST variability in the EEA during boreal summer and excessive, it shows excessive interannual SST variability off the coasts of Angola and Namibia during boreal summer (Figure 1b). CGCMs Prodhomme et al. (2019) showed,

80 using Coupled Model Intercomparison Project (CMIP) phase 5 simulations, that the representation of the Atlantic Niño is strongly linked to the cold tongue development, highlighting the importance to accurately capture the seasonal evolution of the wind stress and SST in CGCMs. CGCMs have been extensively evaluated in the tropical Atlantic region, serving as valuable tools for comprehending and predicting variability patterns (Crespo et al., 2022; Prigent et al., 2023a, b). To our knowledge, relatively little effort has been devoted to the simulation of interannual variability in OGCMs-ocean general circulation models (OGCMs) in the tropical Atlantic. For example, Wen et al. (2017) analysed the response of tropical ocean simulations with two different surfaces forcings: ~~NCEP~~the National Centers for Environmental Prediction/DOE-R2 (Kanamitsu et al., 2002) and CFSR (Saha et al., 2010)DOE reanalysis 2 (NCEP/DOE-R2; Kanamitsu et al., 2002) and the Climate Forecast System Reanalysis (CFSR; Saha et al., 2010). They found that the magnitude of the ocean temperature variability simulated using these two surface forcings was comparable in the tropical Pacific, however, they showed that using CFSR lead to some improvements in the tropical Atlantic, ~~indicating~~emphasising that the improvements in the tropical Atlantic were mainly attributable to differences in surface winds.

The Ocean Model Intercomparison Project (OMIP; Griffies et al., 2016) provides an ideal framework for evaluating the simulation of interannual SST variability in the equatorial Atlantic by ocean models. The main objective of OMIPs is to provide a framework for assessing, understanding and improving the ocean and sea-ice components of global climate models that contribute to the ~~Coupled Model Intercomparison Project (CMIP)~~. ~~OMIP~~CMIP. OMIPs have used two atmospheric and river runoff datasets to force ocean sea-ice models. In OMIP phase 1 (OMIP1; Griffies et al., 2009), the Coordinated Ocean-ice Reference Experiments phase-II atmospheric state (CORE-II; Large and Yeager, 2009), mainly derived from the ~~National Centers for Environmental Prediction (NCEP) atmospheric reanalysis~~NCEP atmospheric reanalysis phase 1, was employed. In OMIP phase 2 (OMIP2; Griffies et al., 2016; Tsujino et al., 2020), the JRA-55 based surface dataset for driving ocean-sea-ice models (JRA-55-do; Tsujino et al., 2018) was used.

100 ~~Compared to ORA-S5 (Figure 1a) over the period January 1985 to December 2004, the OMIP1 ensemble mean overestimates the interannual SST variability in the equatorial Atlantic during boreal summer (Figure 1c), while the OMIP2 ensemble mean underestimates it (Figure 1d). If we extend the time period to the period from January 1970 to December 2004 (Figure S1), relative to ORA-S5, the OMIP1 (OMIP2) ensemble mean still overestimates (underestimates) the MJJ interannual SST variability. When compared to the OMIP1 individual ensemble members over the period from January 1985 to December 2004, the interannual SST variability in the tropical Atlantic during boreal summer is systematically weaker in the OMIP2 ensemble members (Figure S2), raising several questions that we address in the following sections. In particular, In the present study we will address the following questions: how well do OMIP1 and OMIP2 ensembles simulate the ~~seasonal cycles~~monthly climatologies of equatorial Atlantic zonal winds, sea level anomalies (SLA) and SSTs? What are the differences in the interannual SST variability within the EEA between OMIP1 and OMIP2? ~~Is the interannual SST variability in the equatorial Atlantic, as simulated by OMIP models, dependent on the atmospheric forcing used? If so, which~~ Which component of the atmospheric forcing ~~leads to discrepancies in the interannual SST variability~~is responsible for these differences?~~

To address these questions we utilise various observational datasets, reanalysis products, and conduct sensitivity experiments, all of which are detailed in section 2. We scrutinise the seasonal patterns of equatorial Atlantic zonal winds, SLAs and SSTs

in section 3. Section 4 is dedicated to assessing the interannual SST, [SSH](#) and temperature variability within OMIP1 and
115 OMIP2 ensembles. In section 5, we delve into the impact of wind forcing on ~~interannual SST variability in the EEA~~ [the EEA](#)
[interannual variability](#). Final conclusions along with discussions can be found in section 6.

2 Data and methods

2.1 Data

2.1.1 Reanalysis products and observational datasets

120 This study employs several reanalysis products with monthly temporal resolution, if not stated otherwise. Specifically, SST, sea
surface height (SSH), zonal wind stress, and upper 200 m depth ocean [potential](#) temperature are taken from the Ocean Reanaly-
sis System version 5 (ORA-S5; Zuo et al., 2019). ORA-S5 provides data at a horizontal resolution of 0.25° by 0.25° and spans
the period from January 1958 to present day. ORA-S5 has 72 z-levels in the ocean. The Optimum Interpolation SST version 2
(OI-SST, Reynolds et al., 2002) is also used, it is available at a horizontal resolution of 1° by 1° over the period from December
125 1981 to January 2023. Additionally, zonal ~~wind winds~~ at 10 m height (U10) ~~is obtained from various sources, including the~~
~~NCEP/NCAR Reanalysis 1 (NCEP-R1; Kalnay et al., 1996), which is available at a horizontal resolution of 2.5° by 2.5° and~~
~~covers the period from January 1948 to present day, the NCEP/DOE Reanalysis 2 (NCEP/DOE-R2; Kanamitsu et al., 2002)~~
~~, which is available at a horizontal resolution of 2.5° by 2.5° from January 1979 to present day, the fifth generation of the~~
~~European Centre for Medium-Range Weather Forecast (ECMWF) reanalysis (ERA5; Hersbach et al., 2023), with a horizontal~~
130 ~~resolution of 0.25° by 0.25° , spanning the period January 1940 to present day, the~~ [are obtained from the](#) CORE-II [forcing](#)
[atmospheric state](#) (Large and Yeager, 2009), with a horizontal resolution of 2° by 2° and a temporal resolution of 6 hours
encompassing the period from January 1948 to December 2009, and ~~finally from~~ the JRA55-do [atmospheric](#) forcing derived
from the Japanese 55 years Reanalysis (Griffies et al., 2016; Tsujino et al., 2018), with a horizontal resolution of $0.5625^\circ \times$
 0.5625° ($\sim 55 \text{ km} \times 55 \text{ km}$ [at the equator](#)) and a temporal resolution of 3 hours spanning from January 1958 to December
135 2018.

In addition to reanalysis products, ~~one zonal wind~~ [zonal winds](#) at 10 m height ~~dataset is obtained~~ [are taken](#) from the Cross-
Calibrated Multi-Platform version 2 (CCMP v2; Mears et al., 2019), providing data at a horizontal resolution of 0.25° by 0.25°
and spanning from January ~~1987 to December 2015~~ [1988 to December 2017](#). To validate the SLA from the OMIP models, we
compare it to the monthly mean gridded AVISO data version vDT2021 available at a horizontal resolution of 0.25° by 0.25°
140 spanning the period from January 1993 to present.

2.1.2 OMIP data

In this study, we assess how models participating in OMIP1 and OMIP2 simulate ~~interannual SST variability in the tropical~~
~~Atlantic~~ [the equatorial Atlantic interannual variability](#). The OMIP1 protocol consists of five consecutive cycles of the 62-year-
long CORE-II ~~forcing~~ [atmospheric state](#) (Large and Yeager, 2009), whereas the OMIP2 protocol consists of six consecutive

Table 1. OMIP1 models (~~0-5~~0-6) and OMIP2 models (~~6-12~~7-14) used in this study. [The table indicates the model name, the ocean model used as well as the number of grid points in the longitudinal, latitudinal and vertical dimensions.](#)

Num	Model name	Ocean model	Ocean resolution (lon-nlon × lat-nlat × levels-nlevels)
0	CMCC-CM2-SR5	NEMO3.6	362 × 292 × 50
1	CMCC-ESM2	NEMO3.6	362 × 292 × 50
2	EC-Earth3	NEMO3.6	362 × 292 × 75
3	IPSL-CM6A-LR	NEMO-OPA	362 × 332 × 75
4	MIROC6	COCO4.9	360 × 256 × 63
5	MRI-ESM2-0	MRI.COM4.4	360 × 364 × 61
5-6	NorESM2-LM	MICOM	360 × 384 × 70
6-7	ACCESS-OM2	MOM5.1	360 × 300 × 50
7-8	ACCESS-OM2-025	MOM5.1	1440 × 1080 × 50
8-9	CMCC-CM2-HR4	NEMO3.6	1442 × 1051 × 50
9-10	CMCC-CM2-SR5	NEMO3.6	362 × 292 × 50
10-11	EC-Earth3	NEMO3.6	362 × 292 × 75
11-12	MIROC6	COCO4.9	360 × 256 × 63
13	MRI-ESM2-0	MRI.COM4.4	360 × 364 × 61
12-14	NorESM2-LM	MICOM	360 × 384 × 70

145 cycles of the ~~60-year-long~~ [61-year-long](#) JRA55-do forcing. The JRA55-do has a higher temporal resolution (~~3-hours~~ [3 hourly](#)) and finer spatial resolution ($0.5625^\circ \times 0.5625^\circ \sim 55 \text{ km} \times 55 \text{ km}$ [at the equator](#)) than the CORE-II forcing (6 hourly and 2° by 2° , respectively). [Models participating in both OMIPs have used the same ocean model physics.](#) For the purpose of analysis, we focused on the fifth and sixth cycle of OMIP1 and OMIP2, respectively, during a common period from January 1985 to December 2004, aligning with Farneti et al. (2022). ~~Only~~ [All](#) ocean models with a resolution finer than 1° by 1° ~~are considered~~ [in this study and having all the variables needed for this study](#) are listed in Table 1. ~~All~~ [Considered](#) models were bi-linearly interpolated horizontally onto a regular 1° by 1° grid and vertically on the following depth levels: 6, 15, 25, 35, 45, 55, 65, 75, 85, 95, 105, 115, 125, 135, 145, 156.9, 178.4, 222.5, 303.1. The following variables were utilised in the analysis: SST (variable name: TOS), SSH (variable name: ZOS), zonal wind stress (variable name: UAS), ocean temperature (variable name: THETAO), mixed layer depth (variable name: MLOTST), [and](#) net surface heat flux (variable name: HFDS), ~~and ocean vertical~~ [velocity \(variable name: WO\)](#).

150

155

2.1.3 CMIP6 data

~~The eighteen~~ [All fifty five](#) CMIP6 models [from the variant r1i1p1f1](#) considered in Figure 1 are listed in Table S1. We use monthly mean outputs of SST ~~from the variant r1i1p1f1~~ (variable name: TOS) retrieved over the historical period from January 1985 to December 2004. Before analysis, models' outputs were bi-linearly interpolated on a common 1° by 1° [regular](#) grid.

160 2.1.4 Simulations with the GFDL-MOM5 model

We conducted several [modelling](#) experiments to complement the OMIP analyses. We employed the NOAA-GFDL Modular Ocean Model version 5 (MOM5; Griffies, 2012), which is a free-surface primitive equation model and uses a z^* ~~vertical~~ [rescaled geopotential](#) coordinate.

165 First, we performed a control run (MOM5-LR) following the OMIP2 protocol (Griffies et al., 2016), running the MOM5 ocean model for six consecutive cycles of the ~~60-year-long~~ [61-year-long](#) JRA55-do forcing. The simulation was conducted at 1° ~~nominal~~ resolution in the horizontal and [with](#) 50 vertical levels. In MOM5-LR, subgrid mesoscale processes are parameterized with the Gent-McWilliams skew-flux closure scheme (Gent and McWilliams, 1990; Gent et al., 1995; Griffies, 1998) and submesoscale eddy fluxes according to Fox-Kemper et al. (2008) and Fox-Kemper et al. (2011). Vertical mixing is represented with a K-profile parameterization (Large et al., 1994).

170 Next, we examined the ~~relative influence of different wind and heat flux forcing on interannual SST variability in the EEA by designing a suite of sensitivity experiments. The role of surface winds was investigated with MOM5-LR-winds. This experiment mirrors influence of the wind forcing on the MOM5-EEA interannual variability. An additional experiment, MOM5-LR-anom, mirrors the MOM5-LR configuration, with the exception that we repeated the sixth cycle by replacing the JRA55-do winds at 10 m height (U10 and V10) with the a reconstructed wind field. The wind field used in MOM5-LR-anom is the sum of the JRA55-do monthly climatological mean plus the monthly anomalies from the climatological CORE-II wind datasets (Large and Yeager, 2009). Although winds. As turbulent fluxes of momentum, heat and moisture are derived through bulk formulae based on the near surface atmospheric state (including 10 m winds), all surfaces fluxes are expected to be affected by the reconstructed wind field. Also, although not energetically consistent with the other forcing variables, this configuration will provide provides a sensitivity for the upper ocean response to wind foreing. For an investigation into the impact of heat flux forcing on EEA interannual SST variability , we conducted a similar experiment with MOM5-LR-heat. MOM5-LR-heat is similar to MOM5-LR-winds, but in this case the JRA55-do longwave and shortwave heat fluxes are replaced by the the wind variability in the CORE-II heat fluxes over the full sixth cycle. It is worth noting that the latent and sensible heat fluxes in MOM5-LR-heat depend on JRA55-do winds. forcing.~~

175

180

Finally, to assess the impact of the horizontal resolution on the simulation of interannual SST variability in the EEA, we conducted a MOM5-HR experiment following the OMIP2 protocol. MOM5-HR has a similar configuration to MOM5-LR, but its horizontal resolution is refined to 0.25° by 0.25° and the parameterization for mesoscale eddy fluxes is turned off. As for OMIP2 and MOM5-LR, we analysed the sixth cycle of MOM5-HR. [In supplementary Text S1 we have evaluated the outputs of MOM5-LR and MOM5-HR simulations against ORA-S5, focusing on the equatorial Atlantic Ocean mean-state, monthly climatology and interannual temperature variability. This comparison shows that even though MOM5-LR and MOM5-HR feature some biases, both simulations are able to capture reasonably well the tropical Atlantic mean-state, monthly climatology as well as the upper 200 m temperature variability.](#)

185

190

2.2 Methodology

2.2.1 Definition of anomalies

We compare the ~~interannual SST variability in the EEA~~ EEA interannual variability simulated by the OMIP1 ensemble mean to the OMIP2 ensemble mean over a 20-year period spanning from January 1985 to December 2004. Throughout this paper, prior to all analysis, the linear trend is removed pointwise to each dataset. Monthly-mean anomalies are computed by subtracting the climatological monthly-mean seasonal cycle derived over the study period. The boreal summer interannual variability is quantified as the standard deviation of the MJJ-averaged anomalies.

2.2.2 Thermocline depth, mixed layer depth and sea level anomaly definitions

The mean depth of the thermocline is defined as the depth of the maximum vertical temperature gradient (dT/dz). SSH anomalies are used as a proxy for thermocline-depth variations. Mixed layer depth (MLD) is determined as the ocean depth at which the potential density σ_θ has increased by $0.03 \text{ kg}\cdot\text{m}^{-3}$ relative to the top model level value (Griffies et al., 2016). A discussion on the method and its implications in defining MLD in ~~the~~ OMIP models can be found in Treguier et al. (2023). The MLD, dT/dz and corresponding depth of the maximum dT/dz are ~~depicted~~ shown for each OMIP model and sensitivity experiments in Figure ~~S3~~ S1. Sea level anomaly (SLA) is defined as the pointwise difference between the SSH and the mean sea surface, with the mean sea surface calculated as the SSH averaged of the period January 1985 to December 2004. The equatorial Atlantic thermocline tilt is defined as the difference of the depth of the maximum dT/dz between the ATL4 and ATL3 regions.

2.2.3 Bjerknes feedback and thermal damping

The three components of the Bjerknes feedback (BF) are assessed as follows. The first component (BF1) is the linear regression of ATL4-averaged zonal wind stress anomalies in MJJ on ATL3-averaged SST anomalies in MJJ. The second component (BF2) is the linear regression of ATL3-averaged SSH anomalies in MJJ on ATL4-averaged zonal wind stress anomalies in MJJ. The third component (BF3) is the linear regression of ATL3-averaged SST anomalies in MJJ on ATL3-averaged SSH anomalies in MJJ. Additionally, the thermal damping is quantified as the linear regression of ATL3-averaged net heat flux anomalies in MJJ on ATL3-averaged SST anomalies in MJJ.

215 3 Comparison of the OMIP1 and OMIP2 ~~seasonal cycles~~ equatorial Atlantic monthly climatologies

~~In~~ Accurately simulating the equatorial Atlantic wind, SLA and SST monthly climatologies in ocean models is crucial for the good representation of the EEA interannual SST variability (Prodhomme et al., 2019). Therefore, in this section we compare the OMIP1 and OMIP2 ~~ensemble mean seasonal cycles~~ monthly climatological means of the equatorial Atlantic (40°W - 10°E ; 3°S - 3°S) zonal winds, ~~SLA and SST to the~~ SLAs and SSTs to reanalysis products and observational datasets. A comparison to the Prediction and Research Moored Array in the Tropical Atlantic (PIRATA; Servain et al., 1998; Bourlès et al., 2008) at the equatorial moorings of 35°W , 23°W , 10°W , and 0°E can be found in Supplementary Text S2.

The seasonal-cycle-monthly climatology of the zonal wind in the western equatorial Atlantic is dominated by an annual cycle with maximum easterly winds in September-October-November (SON) and minimum easterlies in MAM (Figure 2a). Meanwhile, the EEA zonal wind exhibits a semiannual cycle (Figure 2a) with maxima in ~~Januray-February-March and in~~
225 January-February-March and SON. Both CORE-II (Figure 2b) and JRA55-do (Figure 2c) surface forcings closely mirror the observed seasonal-cycles-monthly climatology of the zonal wind in the equatorial Atlantic. In the ATL4 region (Figure 2d), CORE-II and JRA55-do zonal winds are stronger than those of CCMP v2 throughout the year.

Next, we analyse the seasonal-cycle-monthly climatology of the SLA, where negative (positive) SLA indicates a shoaling (deepening) of the thermocline. Consistent with the strong link between western equatorial Atlantic zonal winds and
230 the thermocline depth (Philander and Pacanowski, 1986), the seasonal-cycle-of-the-equatorial-Atlantic-thermocline-monthly climatology of the SLA depicts an annual cycle in the west ~~and (Figure 2e).~~ In the east, a semiannual cycle ~~in the east (Figure 2d; Ding et al., 2009).~~ appear in the SLA. Brandt et al. (2016) showed that the equatorial Atlantic seasonal cycle of SLA is driven by resonance modes associated with the second and fourth baroclinic modes at semiannual and annual frequencies, respectively. In the western equatorial Atlantic, the thermocline reaches its shallowest point during MAM and this signal pro-
235 gresses eastward, reaching 10°W by July. In SON, the thermocline is deep in the west and the signal also propagates eastward, but its propagation is faster. These eastward propagating SLA signals can be understood in terms of linear dynamics and are essentially explained by the first four baroclinic modes (Ding et al., 2009). ~~In the EEA, a semiannual SLA cycle emerges.~~ Both the OMIP1 (Figure 2ef) and OMIP2 (Figure 2fg) ensemble means exhibit patterns similar to ORA-S5. ~~However~~In comparison to ORA-S5, the amplitude of the annual cycle in the western equatorial Atlantic is ~~weaker in the OMIP2 ensemble mean~~
240 ~~compared to the OMIP1 ensemble mean. Quantitatively, the difference in SLA between SON and MAM, averaged between 40°W and 30°W and from 3°S to 3°N, amounts to 0.096 m, 0.072 ± 0.007 m and 0.053 ± 0.01 m for ORA-S5, OMIP1, and OMIP2 ensemble means, respectively. Hence, too weak in both OMIP ensembles (Table 2). However,~~ relative to the OMIP2 ensemble mean, the annual cycle of the SLA in the western equatorial Atlantic is ~~3540%~~ larger in the OMIP1 ensemble mean. ~~Yet, relative to ORA-S5, both OMIP ensemble means have a too weak SLA annual cycle in the western equatorial Atlantic~~
245 the ATL3 region (Figure 2h) the shoaling of the thermocline in JJA, as indicated by the negative SLA, is about 30% too weak in both OMIP ensembles in comparison to ORA-S5 (Table 2).

The shoaling of the thermocline depth from MAM to JAS in the ATL3 region (Figure 2h) is closely related to the rapid decrease in SST (Figure 2g). ~~For i).~~ In ORA-S5, the ATL3-averaged SST ~~drops by 3.73 °C, decreasing~~ decreases from 28.52 °C in MAM to 24.79 °C in JAS. ~~In the case of the OMIP1 ensemble (Figure 2h), the ATL3-averaged SST drops by 3.18,~~
250 with a cooling of 3.73 °C (Table 2). In comparison to ORA-S5, both OMIP ensemble means (Figures 2j, k) generate a weaker cooling in the ATL3 region (3.19 ± 0.1 °C ; declining from 28.53 for OMIP1 and 3.29 ± 0.05-0.15 °C in MAM to 25.35 ± 0.08 °C in JAS. Similarly, for the for OMIP2 ensemble (Figure 2i), the ATL3-averaged SST decreases by 3.28 ± 0.16 °C, going from 28.65 ± 0.05 °C in MAM to 25.37 ± 0.16 °C in JAS. These numbers indicate that, in comparison to ORA-S5, both OMIP ensemble means generate a weaker cooling from MAM to JAS., Figure 2l) from MAM to JAS. It is noteworthy that the
255 difference in cooling between the OMIP1 and OMIP2 ensemble means is mainly due to slightly warmer ATL3 SSTs in MAM for OMIP2 compared to OMIP1.

Table 2. Table summarising key values allowing for the comparison of OMIP1 and OMIP2 ensemble means to ORA-S5 in the equatorial Atlantic, over the period from January 1985 to December 2004. Values in parenthesis are for JAS.

	<u>ORA-S5/CCMP v2</u>	<u>OMIP1/CORE-II</u>	<u>OMIP2/JRA55-do</u>
<u>SLA 40°W-30°W SON minus MAM (m)</u>	<u>0.096</u>	<u>0.070 ± 0.008</u>	<u>0.050 ± 0.01</u>
<u>ATL3-averaged SLA in JJA (m)</u>	<u>-0.037</u>	<u>-0.028 ± 0.007</u>	<u>-0.029 ± 0.007</u>
<u>ATL3-averaged SST MAM (JAS) (°C)</u>	<u>28.52 (24.79)</u>	<u>28.51 ± 0.07 (25.31 ± 0.12)</u>	<u>28.63 ± 0.06 (25.34 ± 0.17)</u>
<u>Equatorial Atlantic U10 MAM (JAS) (m·s⁻¹)</u>	<u>-1.91 (-2.24)</u>	<u>-1.89 (-2.76)</u>	<u>-1.99 (-2.27)</u>
<u>Equatorial tilt MAM (JAS) (m)</u>	<u>23.30 (44.45)</u>	<u>30.50 ± 3.52 (47.29 ± 3.49)</u>	<u>35.44 ± 3.52 (44.80 ± 3.93)</u>
<u>ATL3 upper 25 m temperature MAM (JAS) (°C)</u>	<u>28.44 (24.67)</u>	<u>28.38 ± 0.07 (25.22 ± 0.15)</u>	<u>28.42 ± 0.12 (25.25 ± 0.19)</u>
<u>ATL3-averaged MLD MAM (JAS) (m)</u>	<u>18.87 (26.26)</u>	<u>16.23 ± 1.45 (23.43 ± 2.94)</u>	<u>13.52 ± 3.36 (25.60 ± 5.69)</u>
<u>ATL3-averaged distance between Z20 and Z24 MAM (JAS) (m)</u>	<u>16.08 (23.23)</u>	<u>34.54 (31.94)</u>	<u>34.65 (30.21)</u>

As the seasonal cycle- As the monthly climatology of the equatorial Atlantic SST is strongly influenced by subsurface conditions, we examined the upper 200 m ocean temperature during both MAM and JAS (Figure 3). During MAM (Figure 3a), the easterly winds in the equatorial Atlantic equatorial Atlantic easterly winds (40°W-10°E; 3°S-3°N) are relatively weak, measuring 1.91 m·s⁻¹ in CCMP v2. Consequently, the thermocline exhibits a small tilt of 23.30 m, with the upper 25 m in the ATL3 region having a temperature of 28.44 °C. Notably, the ATL3-averaged MLD is located at 18.87 m. We note that the vertical temperature gradient is pronounced in this region, with the distance between the 20 °C and 25-24 °C isotherms measuring 19.68 16.08 m. In JAS (Figure 3b), the equatorial Atlantic easterlies intensify to 2.24 m·s⁻¹, leading to a steeper thermocline with a tilt of 44.45 m and an increased slope of the isotherms between 20°W and 0°E. The upper 25 m in the ATL3 experiences a strong cooling, with a temperature of 24.67 °C, while the MLD deepens to 26.26 m.

Comparing the above values to the OMIP1 ensemble mean OMIP ensemble means (Table 2), we observe that the upper 200 m temperature sections in both MAM (Figures 3c and d, e) and JAS (Figures 3e and d, f) align closely with ORA-S5. However, some differences are listed next. In MAM (Figure 3e Figures 3c, e), the CORE-II (JRA55-do) easterlies in the equatorial Atlantic remain weak at 1.89 m·s⁻¹, resulting in a thermocline tilt of 30.36 ± 3.79 m, slightly weaker (stronger) than CCMP v2 and the tilt of the thermocline is overestimated in both OMIP ensembles. The upper 25 m temperature in the ATL3 region exhibit a temperature of 28.40 ± 0.05 °C, and the maximum vertical velocity, found at 35 m depth, amounts to 4.17 ± 0.35 10⁻⁶ m·s⁻¹ (Figure 3d). The ATL3-averaged MLD is located at 16.36 ± 1.53 m. Notably, the is well captured by the OMIP1 and OMIP2 ensemble means but in both ensembles the MLD is too shallow (Table 2). Relative to ORA-S5, both OMIP ensembles feature a too diffusive thermocline as indicated by the large distance between the 20 °C and 25-24 °C isotherms in the ATL3 region is larger (40.61 m) in the OMIP1 ensemble, indicating a more diffusive thermocline (Table 2). In JAS (Figure 3e d, f), the CORE-II easterlies strengthen to 2.76 m·s⁻¹, resulting in a thermocline tilt of 46.64 ± 3.36 m. The upper 25 m temperature in the ATL3 decreases to 25.26 ± 0.11 °C, and the maximum vertical velocity deepens to 55 m depth and strengthens to 5.64 ± 1.12 10⁻⁶

$\text{m}\cdot\text{s}^{-1}$ (Figure 3f) equatorial Atlantic easterlies are overestimated in both ensembles, however, the tilt of the thermocline in the OMIP ensembles is close to the one from ORA-S5 (Table 2). The ATL3-averaged MLD deepens to 23.91 ± 2.92 m.

280 We next focus on the OMIP2 ensemble mean (Figures 3g-j). In MAM (Figures 3g-h), the JRA55-do easterlies in the equatorial Atlantic, measuring $1.99 \text{ m}\cdot\text{s}^{-1}$, are stronger than the CORE-II ones, leading to a larger thermocline tilt of 35.04 ± 3.72 m. The ATL3-averaged upper 25 m temperature reaches to 28.44 ± 0.12 °C, and the MLD is located at 13.90 ± 3.44 m. More importantly, the distance between the 20 °C and the 25 °C remains substantial at 41.13 m. The maximum vertical velocity from the OMIP ensemble means in the ATL3 (Figure 3h), situated at 35 m depth, is $4.24 \pm 0.74 \cdot 10^{-6} \text{ m}\cdot\text{s}^{-1}$. In JAS (Figure 285 3f), is not cooling as much as in ORA-S5 (Table 2). Finally, the deepening of the JRA55-do easterlies strengthen to $2.27 \text{ m}\cdot\text{s}^{-1}$, resulting in a thermocline tilt of 44.03 ± 3.59 m. The upper 25 m ATL3 temperature decreases to 25.28 ± 0.19 °C and the maximum vertical velocity deepens to 45 m depth but weakens slightly to $4.19 \pm 1.23 \cdot 10^{-6} \text{ m}\cdot\text{s}^{-1}$. The ATL3-averaged MLD deepens to 26.20 ± 5.84 m. We note that the 25 °C isotherm is not tilting as much as in the OMIP1 ensemble mean, consistent with differences in vertical velocities within the ATL3 region (Figures 3h, j), is better represented in the OMIP2 ensemble than 290 in the OMIP1 ensemble (Table 2).

To summarise this section and answer the first of our questions question raised in the introduction, we find that the OMIP1 and OMIP2 ensemble means closely replicate the seasonal cycles monthly climatologies of equatorial Atlantic zonal winds, SSTs, SLAs and upper 200 m ocean temperatures when compared to ORA-S5 and CCMP v2. Nonetheless, we highlight some discrepancies relative to ORA-S5: (1) the annual cycle of the SLA in the western equatorial Atlantic is seasonal shoaling of 295 the thermocline in JJA is about 30% weaker in both OMIP ensemble means, but the OMIP1 ensemble mean annual cycle of the SLA in the western equatorial Atlantic is 35% larger than the one of the OMIP2 ensemble mean; (2) both OMIP ensemble means exhibit a too diffusive thermocline; (3) the cooling of the SST and upper 25 m ocean temperature from MAM to JAS in the ATL3 is less pronounced in the OMIP ensemble means; (4) the equatorial upwelling in JAS appears to be weaker in both OMIP ensemble means.

300 4 Comparison of OMIP1 and OMIP2 equatorial Atlantic interannual variabilities

The interannual variability in the equatorial Atlantic exhibits a pronounced seasonality (Keenlyside and Latif, 2007; Lübbecke et al., 2018). Specifically, high interannual zonal wind variability in CCMP v2 in the western equatorial Atlantic occurs from 40°W to 20°W during April-May-June (Figure 4a) and from 20°W to 15°W in March and April. As OMIP1 and OMIP2 models are forced by the CORE-II and JRA55-do 10 m winds, respectively, we compare them to CCMP v2. The CORE-II 305 zonal wind forcing displays a similar pattern to CCMP v2 from 40°W to 20°W but with weaker interannual variability (Figure 4b). The JRA55-do forcing also exhibits a similar pattern of interannual zonal wind variability but underestimates it in April-May-June (Figure 4c). Additionally, the JRA55-do forcing (Figure 4c) reveals high zonal wind variability between 10°W and 10°E in January and February, which is not as prominent in CCMP v2 (Figure 4a) and absent in the CORE-II forcing (Figure 4b). Quantitatively, the standard deviation of AMJ-averaged U10 anomalies in the ATL4 region is $0.80 \text{ m}\cdot\text{s}^{-1}$ for CCMP v2 310 over the period from January 1988 to December 2004 and $0.70 \text{ m}\cdot\text{s}^{-1}$ and $0.68 \text{ m}\cdot\text{s}^{-1}$ for CORE-II and JRA55-do over the

period from January 1985 to December 2004, respectively. [The ATL4-averaged monthly climatological standard deviation of the U10 anomalies \(Figure 4d\)](#) reveals that the peak zonal wind variability is in May for CORE-II and in April for JRA55-do and CCMP v2.

Typically, sudden relaxation (intensification) of the Trade winds in the western equatorial Atlantic can trigger interannual downwelling (upwelling) equatorial Kelvin waves ([Imbol-Koungue et al., 2017](#))([Illig et al., 2004](#)). While propagating eastward along the equatorial wave guide, these waves generate thermocline-depth variations which can be observed in the SSH anomalies. In the following, we compare the [equatorial Atlantic](#) interannual SSH variability in OMIP1 and OMIP2 ensemble means to ORA-S5. In ORA-S5, two peaks of interannual SSH variability are observed during boreal summer, one between 40°W and 35°W and another between 20°W and 0°E (Figure 4de). Additionally, ORA-S5 exhibits high interannual SSH variability in November-December in the EEA (Figure 4de). The interannual SSH variability in the ATL3 region is ~~considerably stronger~~ [too strong \(weak\)](#) in the OMIP1 (~~OMIP2~~) ensemble mean compared to ~~the OMIP2 ensemble mean~~ ORA-S5 (Figure 4e, ff, g, h). In numbers, the OMIP1 (OMIP2) ensemble mean ATL3-averaged [interannual](#) SSH variability in MJJ is $0.02 \pm 0.001 \text{ m}$ (~~0.014-0.002 m~~ ($0.015 \pm 0.001-0.002 \text{ m}$)), while it is 0.019 m in ORA-S5 (Figure 4h). The anomaly correlation coefficients and root-mean-square errors between OMIP1 and OMIP2 ~~simulations ensemble means~~ with AVISO SLA, evaluated over the period January 1993 to December 2004, are shown in Figures ~~S4a-d, respectively~~ [S2a-d](#). These figures exhibit high correlation (>0.75 , Figures ~~S4a~~[S2a](#), b) and low root-mean-square error ($<0.01 \text{ m}$, Figures ~~S4e~~[S2c](#), d) in the EEA for both ~~OMIP1 and OMIP2~~ [OMIP](#) ensemble means, indicating a ~~good-high~~ fidelity of the OMIP ensembles with AVISO. To further illustrate that, we show the timeseries depicting ATL3-averaged SSH anomalies for AVISO, OMIP1, and OMIP2 ensemble means in Figure ~~S4e~~[S3e](#). Despite robust correlations between both OMIP ensembles and AVISO (~~0.79 for OMIP1 and 0.78 for OMIP2~~), evaluated over the period from January 1993 to December 2004, the amplitude of the monthly mean SSH anomalies is larger in OMIP1 compared to OMIP2. This indicates that thermocline depth variations are larger in the OMIP1 ensemble mean compared to the OMIP2 ensemble mean.

Finally, we compare the [equatorial Atlantic](#) interannual SST variability ~~in the equatorial Atlantic~~ from the OMIP1 and OMIP2 ensemble means to ORA-S5. ORA-S5 displays two peaks of interannual SST variability in the ATL3 region, one in MJJ and ~~one another~~ in November-December (Figure 4gi). Both OMIP ensemble means exhibit a similar pattern to ORA-S5. However, relative to ORA-S5, the OMIP1 (OMIP2) ensemble mean overestimates (underestimates) the MJJ interannual SST variability [in the EEA](#) (Figure 4h, ij, k). In numbers, the standard deviation of the MJJ-averaged SST anomalies in the ATL3 region is $0.62 \pm 0.04 \text{ }^\circ\text{C}$, $0.41 \pm 0.03 \text{ }^\circ\text{C}$ and $0.59 \text{ }^\circ\text{C}$ for the OMIP1 and OMIP2 ensemble means and ORA-S5, respectively. The [equatorial Atlantic interannual SST variability in MJJ is systematically larger in OMIP1 ensemble members than in OMIP2 ensemble members \(Figure S3\)](#). The anomaly correlation coefficients and root-mean-square errors between OMIP1 and OMIP2 simulations with OI-SST, evaluated over the period January 1985 to December 2004, are shown in Figures ~~S5a-d, respectively~~ [S4a-d](#). In comparison to the tropical Atlantic ocean, the EEA and southeastern tropical Atlantic display the lowest anomaly correlation and greatest root-mean-square errors across both OMIP1 and OMIP2 ensembles. This indicates that these regions exhibit the most pronounce ~~disparities~~ [biases](#) between both OMIP ensembles and OI-SST. Nevertheless, it is important to highlight that despite these differences, the anomaly correlation coefficient is high (≈ 0.8 , [Figures S4a, b](#)) and

the root mean-square error is low (<0.5 °C, [Figures S4c, d](#)). To elaborate on this point we present the timeseries depicting the ATL3-averaged SST anomalies for [ORA-S5OI-SST](#), OMIP1, and OMIP2 ensemble means in [Figure S5eS4e](#). Both OMIP1 and OMIP2 ensemble means are highly correlated to OI-SST with Pearson correlation coefficients of 0.79 and 0.80, respectively. However, the [amplitude of the ATL3-averaged SST anomalies in the ATL3 region in the OMIP1 ensemble mean](#) are in general
350 larger than in the OMIP2 ensemble mean.

Ocean-atmosphere interactions are key drivers of the interannual SST variability within the EEA (Jouanno et al., 2017). To delve into this, we examined the various components of the Bjerknes feedback and thermal damping in ORA-S5, along with the ensemble means of OMIP1 and OMIP2 (Figure 5) over the period January 1985 to December 2004. [The first component of the Bjerknes feedback is not discussed given that in a forced ocean model simulation, there is no response of the western equatorial Atlantic winds to the SST anomalies in the eastern equatorial Atlantic.](#) In comparison to ORA-S5 ($0.91 \cdot 10^{-2} \text{ N}\cdot\text{m}^{-2}\cdot\text{°C}^{-1}$),
355 [the BF1 \(Figure 5a\) is overestimated in both OMIP1 \(\$1.05 \pm 0.05 \cdot 10^{-2} \text{ N}\cdot\text{m}^{-2}\cdot\text{°C}^{-1}\$ \) and OMIP2 \(\$1.23 \pm 0.15 \cdot 10^{-2} \text{ N}\cdot\text{m}^{-2}\cdot\text{°C}^{-1}\$ \).](#) Notably, [for which the BF1 is larger in the OMIP2 ensemble than in the OMIP1 ensemble, but the latter has a narrower spread.](#) Turning to the BF2 (Figure 5b) it amounts to $1.79 \text{ m}\cdot(\text{N}\cdot\text{m}^{-2})^{-1}$ in ORA-S5 and is overestimated (underestimated) in, the OMIP1 (OMIP2) ensemble [overestimates \(underestimates\) it](#) with a slope of $1.88 \cdot 1.96 \pm 0.11 \cdot 0.22$
360 $\text{m}\cdot(\text{N}\cdot\text{m}^{-2})^{-1}$ ($1.55 \cdot 1.63 \pm 0.21 \cdot 0.30 \text{ m}\cdot(\text{N}\cdot\text{m}^{-2})^{-1}$). Regarding the BF3 (Figure 5eb), it equals to $26.51 \text{ °C}\cdot\text{m}^{-1}$ for ORA-S5 and to $29.34 \cdot 28.62 \pm 1.8 \cdot 2.42 \text{ °C}\cdot\text{m}^{-1}$ and $26.10 \cdot 25.60 \pm 1.1 \cdot 1.67 \text{ °C}\cdot\text{m}^{-1}$ for the OMIP1 and OMIP2 ensembles, respectively. Hence, the subsurface-surface coupling is more pronounced in the OMIP1 ensemble mean than in the OMIP2 ensemble mean. Lastly, the thermal damping is assessed (Figure 5dc). While ORA-S5 depicts a strong thermal damping ($-21.58 \text{ W}\cdot\text{m}^{-2}\cdot\text{°C}^{-1}$) both OMIP ensemble ensembles underestimate it, with slopes of $-12.18 \cdot -12.47 \pm 1.72 \cdot 1.74 \text{ W}\cdot\text{m}^{-2}\cdot\text{°C}^{-1}$ and $-10.02 \cdot -10.48 \pm$
365 $2.34 \cdot 2.5 \text{ W}\cdot\text{m}^{-2}\cdot\text{°C}^{-1}$ for the OMIP1 and OMIP2 ensembles, respectively.

The contrast between the interannual variability [of the equatorial Atlantic](#) in the OMIP1 and OMIP2 ensemble means extends beyond the surface, as illustrated by the upper 200 m temperature variability in MJJ (Figure 6). In ORA-S5 (Figure 6a), [the maximum two maxima of interannual temperature variability in MJJ occurs are observed in MJJ, one between 40° W and 30° W and from another between 20° W and 0° E within ± 10 m range around the mean thermocline.](#) The [high standard deviation of the ORA-S5 equatorial Atlantic SSH anomalies in MJJ mirrors the upper 200 m interannual temperature variability.](#) The high
370 [interannual temperature variability in the western equatorial Atlantic is situated at a depth of 90 m, making it too deep to influence reach the MLD and, hence, affect the SST.](#) In contrast, the maximum temperature variability in the EEA is located at 50 m depth, [close closer](#) to the MLD, with an average of 1.28 °C for ORA-S5 when considering the ATL3 region and a $\pm 10 \text{ m}$ range around the mean thermocline. [In MJJ, the The MJJ interannual temperature variability in the EEA for the OMIP1 ensemble mean equatorial Atlantic for the OMIP ensemble means](#) (Figure 6b) [features, c\) exhibits](#) a similar pattern to ORA-S5 but with generally weaker [interannual temperature variability.](#) [The standard deviation of the MJJ-averaged temperature anomalies within ± 10 m of the mean thermocline for the ATL3 region in the OMIP1 ensemble mean is \$0.77 \pm 0.06 \text{ °C}\$.](#) The OMIP2 ensemble mean (Figure 6c) also follows a similar pattern to ORA-S5 but displays even less interannual temperature variability in [For both OMIP ensembles, the MJJ equatorial Atlantic interannual SSH variability mirrors the upper 200 m](#)
380 [during MJJ compared to the OMIP1 ensemble mean \(Figure 6b\) interannual temperature variability.](#) The standard deviation of

the MJJ-averaged temperature anomalies within ± 10 m of the mean thermocline for the ATL3 region ~~in the OMIP2 ensemble mean is~~ 0.78 ± 0.06 °C and $0.58 \pm 0.08-0.07$ °C ~~for the OMIP1 and OMIP2 ensembles, respectively~~. The upper 200 m ~~interannual~~ temperature variability in the EEA during MJJ is systematically larger in ~~the~~ OMIP1 ensemble members compared to ~~the~~ OMIP2 ensemble members as shown in Figure S6S5. Given that both OMIP ensemble means exhibit a similar vertical
385 temperature gradient during boreal summer within ± 10 m of the mean thermocline in the ATL3 region, ~~which is amounting to~~ -0.15 ± 0.001 °C·m⁻¹, it can be inferred that the disparities in ~~the equatorial Atlantic~~ interannual temperature variability are primarily driven by larger fluctuations in the thermocline depth. In contrast, the boreal summer vertical temperature gradient for ORA-S5 within ± 10 m of the mean thermocline in the ATL3 region is -0.25 °C·m⁻¹, which can account for its substantially higher subsurface temperature variability.

390 In response to ~~our second question, related to differences in interannual SST variability in EEA within OMIP1 and OMIP2, we observed the second question raised in the introduction, we showed~~ that during the period January 1985 to December 2004, the OMIP1 ensemble exhibits ~~about 51% (34%)~~ greater boreal summer interannual SST ~~and temperature (temperature)~~ variability in the ATL3 region compared to the OMIP2 ensemble. ~~Over the same period and relative to the OMIP2 ensemble, the OMIP1 ensemble has about 33% greater interannual SSH variability in MJJ in the ATL3 region.~~ When contrasting the
395 two ensembles, the OMIP1 ensemble displays a stronger BF2 and BF3, which could account for the larger interannual SST variability. However, the ~~BF1 component is larger in OMIP2, while the~~ thermal damping is more prominent in the OMIP1 ensemble ~~than in the OMIP2 ensemble~~. In the next section, we investigate the impact of the ~~wind forcing on interannual variability in the EEA CORE-II and JRA55-do wind forcings on the EEA interannual variability.~~

5 Influence of the wind forcing on the equatorial Atlantic interannual variability

400 Wind forcing is an important driver ~~of for~~ the equatorial Atlantic mean-state, ~~seasonal cycle~~ and interannual variability (Richter et al., 2012; Wahl et al., 2011). Wen et al. (2017) investigated the response of ~~the~~ tropical ocean simulations to NCEP/DOE-R2 and CFSR surface fluxes ~~. Using sensitivity experiments run and, using sensitivity experiments~~ with the GFDL MOM version 4p1 (Griffies, 2009), they found that prescribing CFSR surface fluxes instead of NCEP/DOE-R2 surface fluxes was significantly improving the simulation of the SST and SSH variabilities in the tropical Atlantic ocean. ~~This underscores the~~
405 ~~sensitivity of the simulation of the tropical Atlantic interannual variability to surface forcings. In Figure 7, we compare different wind reanalysis products over the period from January 1985 to December 2004. All of these reanalyses depict a similar seasonal cycle, characterised by the weakest winds in March and April, followed by a strengthening of the easterly winds from May to December. Notably, NCEP-R1 displays consistently weaker easterlies throughout the year (Figure 7a). Taking the CCMP v2 climatology as a reference, the root mean square error of the climatology is 0.39 m·s⁻¹ for CORE-II and is 0.27 m·s⁻¹ for JRA55-do. When examining zonal wind variability in the western equatorial Atlantic, the amplitude of zonal wind variability between CORE-II and JRA55-do is relatively similar, but JRA55-do reaches its peak in April, while CORE-II's peak occurs in May (Figure 7b). The examination of extended timeseries of zonal wind anomalies in the ATL4 region for both the JRA55-do (over the period 1958 to 2022) and the CORE-II (over the period 1948 to 2007), shows that both forcing~~

415 datasets of their maximum variability in May (Figure S7). This highlights that the disparity in the timing of the peak of the zonal wind variability between JRA55-do and CORE-II (Figure 7b) within the ATL4 region is linked to the specific time periods under consideration. ERA5 depicts the largest zonal wind variability and peaks in April. Both NCEP/DOE-R2 and NCEP-R1 exhibit the smallest zonal wind variability, with both reaching their peaks in May. Taking the CCMP v2 seasonal cycle of the zonal wind variability as a reference, the root-mean-square error for CORE-II is $0.15 \text{ m}\cdot\text{s}^{-1}$ and it is $0.09 \text{ m}\cdot\text{s}^{-1}$ for JRA55-do. The correlation matrix, spanning January 1985 to December 2004, shows the Pearson correlation coefficients between the ATL4-averaged zonal wind anomalies from the different reanalysis datasets (Figure S8). Specifically, it shows that the Pearson correlation coefficient between CCMP v2 and CORE-II is 0.81, while it is 0.89 for JRA55-do (Figure S8). In addition, the Pearson correlation coefficients for ERA5 in relation to CORE-II and JRA55-do are 0.82 and 0.90, respectively (Figure S8). Additionally, we note that JRA55-do, ERA5 and NCEP/DOE-R2 have a secondary peak in February (Figure 7b), whereas this secondary peak is notably weaker in CORE-II and NCEP-R1. In comparison to the CORE-II forcing, the peak of zonal wind variability during February found in the JRA55-do forcing results from a few strong events occurring between 1985 and 2004 (Figure S9a). Figures S9b and S9c depict zonal wind anomalies in the western equatorial Atlantic for April and May, respectively. These figures highlight that zonal winds anomalies in April are more pronounced in JRA55-do compared to CORE-II, while the reverse is observed in May.

430 Western equatorial Atlantic U10 seasonal cycles for the period from January 1985 to December 2004. (a) Seasonal cycle of U10 winds averaged over the ATL4 region. (b) Seasonal cycle of the standard deviation of U10 anomalies averaged over the ATL4 region. Different lines correspond to various reanalysis products: (black) CORE-II, (blue) JRA55-do, (red) ERA5, (cyan) NCEP/DOE-R2, (purple) NCEP-R1, and (orange) CCMP v2. (c, d) Standard deviation of U10 anomalies over the tropical Atlantic during AMJ for JRA55-do and CORE-II respectively.

435 Consequently, in the following, we aim to examine the hypothesis that the different interannual SST equatorial Atlantic interannual variabilities observed in the OMIP ensemble means are a direct consequence of the discrepancies in wind forcing. A comparison of the CORE-II and JRA55-do reanalyses to other reanalysis products can be found in supplementary Text S3. To investigate this, we employ two additional simulations, namely MOM5-LR and MOM5-LR-winds MOM5-LR-anom, as described in section 2.1.4 and compared in Figure 87.

440 Both MOM5-LR (Figure 87a) and MOM5-LR-winds MOM5-LR-anom (Figure 7b) depict high boreal summer interannual SST variability within the ATL3 region. Yet, the MOM5-LR-winds MOM5-LR-anom simulation exhibits a larger interannual SST variability, amounting to 0.59 0.62 °C, in contrast to 0.42 °C for MOM5-LR. This implies that solely replacing JRA55-do winds monthly wind anomalies with CORE-II winds monthly wind anomalies results in a 4048% increase in the EEA interannual SST variability in the EEA. The equatorial Atlantic SSH variability in boreal summer also depicts an increase in MOM5-LR-anom (Figure 7d) relative to MOM5-LR (Figure 7c). Furthermore, this increase is not limited to the surface, as it is also reflected in the upper 200m- m interannual temperature variability during boreal summer. Specifically, the MJJ interannual temperature variability within a ± 10 m range around the mean thermocline is 0.49 °C for MOM5-LR (Figure 8e) and 0.71 0.74 °C for MOM5-LR-winds (Figure 8d) MOM5-LR-anom (Figure 7f). Hence, using CORE-II instead of

~~JRA55-do winds~~ monthly wind anomalies leads to a ~~45~~51% increase in boreal summer interannual temperature variability in the ATL3 region and within ± 10 m of the mean thermocline.

450 The impact of the wind forcing on ~~interannual SSH variability is~~ the equatorial Atlantic interannual variability is further examined in Figure 98. In comparison to MOM5-LR (Figure 98a), ~~MOM5-LR winds~~ (Figure 9) ~~MOM5-LR-anom~~ (Figure 8b) exhibits a similar pattern of equatorial Atlantic interannual SSH variability, albeit with a larger magnitude. Quantitatively, the standard deviation of MJJ-averaged SSH anomalies in the ATL3 region amounts to 0.015 m for MOM5-LR and ~~0.017~~0.020 m for ~~MOM5-LR winds~~ MOM5-LR-anom. Furthermore, there ~~is~~ seems to be a shift of ~~one month from June to~~ July of the maximum ~~about one month of the~~ interannual SSH variability in the EEA ~~when comparing Figures 8a and 8b.~~ The monthly climatological standard deviation of the ATL3-averaged SSH anomalies (Figure 8c) shows that even though MOM5-LR and MOM5-LR-anom both peaks in June, the interannual SSH variability is stronger in May in MOM5-LR than in MOM5-LR-anom and the opposite in July. This temporal shift of about one month in the EEA interannual SSH variability could be related to the different peaks in zonal wind variability in the ATL4 region ~~for~~ between JRA55-do (April) and CORE-II (May).

460 As ~~discussed previously~~ previously discussed, we also find increased interannual SST variability in ~~MOM5-LR winds~~ (Figure 9) ~~MOM5-LR-anom~~ (Figure 8d) relative to MOM5-LR (Figure 9e8e). As for the ATL3 interannual SSH variability, a shift of ~~one month from June to July~~ about one month is also observed in the interannual SST variability ~~in MOM5-LR winds~~ when comparing MOM5-LR to MOM5-LR-anom (Figure 8f).

~~This section allows~~ This section allowed us to answer the last question raised in the introduction. ~~We have demonstrated~~ Namely, we have shown that the surface forcing, and in particular the wind forcing variability, has a significant impact on the ~~interannual SST variability in the equatorial Atlantic~~ equatorial Atlantic interannual variability. Indeed, ~~substituting replacing~~ the JRA55-do ~~winds~~ monthly wind anomalies by the CORE-II ~~winds in MOM5-LR~~ monthly wind anomalies results in a substantial ~~40%~~ increase in ATL3 interannual SST (48%), SSH (33%) and temperature (51%) variability during MJJ, rising from 0.42 °C, 0.015 m, and 0.49 °C for MOM5-LR to ~~0.59~~ 0.62 °C ~~for MOM5-LR winds~~, 0.020 m, and 0.74 °C for ~~MOM5-LR-anom~~.

470 MOM5-LR-anom.

6 Conclusions and discussions

6.1 Conclusions

In this study, we have compared the ~~seasonal cycle~~ monthly climatologies of equatorial Atlantic zonal wind, SLA, and SST ~~between from~~ the OMIP1 and OMIP2 ensemble means and to ORA-S5. Furthermore, we ~~conducted an investigation into the~~ interannual variability of the EEA ~~examined the equatorial Atlantic interannual variability~~ within the OMIP models. Finally, we delved into the causes behind the distinct ~~interannual SST variability~~ equatorial Atlantic interannual variabilities during boreal summer in OMIP1 and OMIP2 ensembles using sensitivity experiments. We have ~~demonstrated shown~~ that over the period from January 1985 to December 2004:

- 480 – The seasonal climatological patterns of the equatorial Atlantic zonal wind, SLA, SST, and ocean temperature in OMIP1 and OMIP2 ensemble means resemble those in ORA-S5. However, some discrepancies are evident: the annual cycle of the SLA in the western equatorial Atlantic is ~~weaker~~ too weak in both OMIP ensemble means, but the OMIP1 ensemble mean annual cycle of the SLA in the western equatorial Atlantic is ~~35~~ about 40% larger than the one of the OMIP2 ensemble mean; the seasonal shoaling of the thermocline in the ATL3 region during JJA is about 30% too weak in the OMIP ensembles in comparison to ORA-S5; both OMIP ensembles have a too ~~diffuse~~ diffusive thermocline; the
- 485 seasonal cooling of SST from MAM to JAS is insufficient in both OMIP ensembles (Figure 2); ~~and the OMIP2 ensemble mean maximum vertical ocean velocity in JAS is weaker than in the OMIP1 ensemble mean. Regarding the too diffuse thermocline, Zhang et al. (2022) using sensitivity experiments, showed that reducing the background diffusivity to better match with microstructure profiles, leads to significant improvements of the subsurface temperature in the equatorial Atlantic.~~
- 490 – In ~~boreal summer and in~~ the ATL3 region during boreal summer, the OMIP1 ensemble mean depicts a 51% greater interannual SST variability and a ~~33% larger~~ 34% larger interannual temperature variability at the thermocline level compared to the OMIP2 ensemble mean (Figure ~~109~~a).
- In boreal summer, both OMIP ensembles exhibit a comparable magnitude of dT/dz in the ATL3 region (Figure ~~109~~b). This suggests that, relative to the OMIP2 ensemble, heightened interannual SST and temperature variability in the OMIP1
- 495 ensemble cannot be attributed to differences in the magnitude of dT/dz .
- ~~Substituting the CORE-II winds for the~~ Replacing the JRA55-do winds in MOM5-LR, an OMIP2-like model, monthly wind anomalies for the CORE-II monthly wind anomalies results in a ~~40~~ 48% increase in ATL3 boreal summer interannual SST variability and a ~~45~~ 51% increase in ~~temperature variability~~ interannual temperature variability at the thermocline level, as depicted in Figure ~~109~~a. This underscores the critical role of the wind forcing in accurately simulating ~~interannual SST variability in the EEA~~ the equatorial Atlantic interannual variability within ocean models. It ~~'s~~ is worth noting that, in comparison to MOM5-LR, the magnitude of dT/dz in ~~MOM5-LR-winds~~ MOM5-LR-anom remains unchanged (Figure ~~109~~b).
- In boreal summer, the equatorial Atlantic thermocline tilt within OMIP models varies between 24 m and 39 m, while it reaches 30 m in the case of ORA-S5 (Figure ~~109~~c). No correlation between the thermocline tilt and the ATL3 interannual SST variability is observed in OMIP models. It is worth noting that both MOM5-LR and ~~MOM5-LR-winds~~ MOM5-LR-anom exhibit a similar thermocline tilt, suggesting that the increased ATL3 interannual SST variability in ~~MOM5-LR-winds~~ MOM5-LR-anom is not attributable to a change in the thermocline tilt (Figure ~~109~~c).
- During AMJ, the zonal wind stress variability in the western equatorial Atlantic is slightly more pronounced in the OMIP1 ensemble mean compared to the OMIP2 ensemble mean. This difference may have played a role in the heightened interannual SST variability observed in ATL3 within the OMIP1 ensemble mean (as illustrated in Figure ~~109~~d). It
- 510

is important to stress that the peak in ATL4 zonal wind variability occurs in April for the JRA55-do forcing and in May for the CORE-II forcing.

515 – In boreal summer, the interannual SSH variability in the ATL3 region is ~~43~~about 33% greater in the OMIP1 ensemble mean compared to the OMIP2 ensemble mean (Figure ~~109~~e). Sensitivity experiments reveal that this change in ATL3 interannual SSH variability from the OMIP1 ~~ensemble~~ to the OMIP2 ensemble is mainly attributed to ~~the wind forcing.~~ Furthermore wind anomalies from the CORE-II forcing. Indeed, when comparing MOM5-LR to ~~MOM5-LR-winds,~~ the MOM5-LR-anom, the interannual SSH variability in the ATL3 region during boreal summer is heightened by ~~133~~33%, as depicted in Figures ~~9 and 108~~ and 9f.

520 In summary, this study has shown, by comparing the OMIP1 and OMIP2 ensembles and by using sensitivity experiments, that seemingly minor uncertainties in the atmospheric ~~forcings~~ forcing can lead to notable discrepancies in the simulated ~~interannual variability in the EEA region~~ equatorial Atlantic interannual variability. For the equatorial Atlantic, we have shown that the interannual variability in ocean models is particularly sensitive to the wind forcing, in line with ~~the~~ results from Wen et al. (2017).

6.2 Discussion

525 It could be argued that changes in ocean model physics from OMIP1 to OMIP2 could also have lead to discrepancies in the simulation of the interannual variability in the equatorial Atlantic. However, models participating in both OMIPs have used the same ocean model physics. Hence, discrepancies in the interannual ~~SST~~ variability in the EEA should be rooted in the atmospheric forcing. The simulation of ~~interannual variability in the EEA region~~ the EEA interannual variability by ocean models may be influenced by several factors other than the wind forcing. Beyond the zonal and meridional winds, the forcing
530 from CORE-II and JRA55-do includes shortwave and longwave heat fluxes, precipitation, river runoff, air temperature at 2 m and evaporation.

~~The impact of shortwave and longwave heat flux forcing on interannual SST and temperature variability in the EEA has been examined using the MOM5-LR-heat sensitivity experiment. In MOM5-LR-heat, the JRA55-do heat fluxes were replaced by CORE-II heat fluxes during the last cycle. MOM5-LR-heat shows only slightly larger interannual SST and temperature variability in the ATL3 region compared to MOM5-LR (Figure S10). This suggests that shortwave and longwave heat flux forcing can only explain a small fraction of the increased interannual SST and temperature variability in the OMIP1 ensemble mean relative to the OMIP2 ensemble mean (Figure S10). However, the~~ However, their relative impact on the ~~simulation of interannual temperature and SST variability in the EEA by precipitation, river runoff, 2-m air temperature and evaporation~~ equatorial Atlantic interannual variability has not been investigated in this study and would require further model experiments and analysis.
540

~~The influence of the ocean horizontal resolution~~ Another factor potentially impacting on the simulation of ~~EEA interannual SST variability by ocean models under JRA55-do forcing has also been examined~~ the EEA is the ocean horizontal resolution. Model pairs such as ACCESS-OM2 and ACCESS-OM2-025, MOM5-LR and MOM5-HR, as well as CMCC-CM2-HR4 and

CMCC-CM2-SR5, were compared to each other. Each model pair has the same number of vertical levels but ~~different horizontal~~
545 ~~resolution: they differ in their horizontal resolution, going from coarse (1° by $^\circ \times 1^\circ$ and) to refined (0.25° by $^\circ \times 0.25^\circ$).~~
This comparison, based only on three model pairs, suggests that increasing the ocean horizontal resolution does not lead to
consistent changes in the equatorial Atlantic mean-state and interannual SST variability in boreal summer (Figure 109). One
notable change is the increase of the vertical ocean temperature gradient and subsurface temperature variability in boreal
summer when comparing MOM5-LR to MOM5-HR (Figure 9b). However, this change is not observed in the other two model
550 pairs. A larger number of model pairs would be required to properly assess the impact of horizontal resolution, and ideally
also vertical resolution, on stratification biases. Finally, we note that both OMIP1 and OMIP2 ensembles are largely biased
towards Eulerian vertical coordinate models, whereas a larger representation of models making use of Lagrangian vertical
coordinates, or generalized vertical coordinates using the vertical Lagrangian-remap method (Griffies et al., 2020), such as
MOM6 (Adcroft et al., 2019) and HYCOM (Bleck, 2002), could be extremely beneficial to the ocean modelling community.
555 ~~Our findings underscore~~ To conclude, our study has underscored the importance of the wind forcing in modelling the inter-
annual variability of the equatorial Atlantic. ~~Therefore~~ As a consequence, it is ~~advisable~~ imperative to sustain and enhance wind
observations in the tropical Atlantic in order to improve the quality of the reanalysis products. ~~In addition, our~~ in the region.
We note that Taboada et al. (2019) conducted a comparative study of different wind reanalysis products and highlighted the
lack of agreement among them in the tropics. Our results suggest that even though the ~~seasonal cycle~~ monthly climatology
560 of the equatorial Atlantic winds is relatively well captured by reanalysis datasets, ~~the interannual variability of the wind~~ their
interannual variability needs more validation in the tropical Atlantic. ~~Taboada et al. (2019) conducted a comparative study of~~
~~different reanalysis products and highlighted the lack of agreement among them in the tropics.~~
~~With respect to the CORE-II atmospheric state (Large and Yeager, 2009), the~~
Finally, the use of JRA55-do ~~surface dataset (Tsujino et al., 2018) seem~~ forcing (Tsujino et al., 2018) within OGCMs seems
565 to improve the simulation of SST variability in ~~extratropical areas and upwelling regions in OGCMs (Figure ??), likely~~
eddy-rich regions like the Gulf Stream, Kuroshio, Malvinas and Agulhas currents as well as in eastern boundary upwelling
systems (Figure 10), probably also due to its higher temporal and spatial resolution ~~compared to the CORE-II atmospheric~~
state (Large and Yeager, 2009). However, the use of the JRA55-do ~~surface dataset results in weak interannual SST variability~~
~~atmospheric forcing results in a weak SST variability~~ not only in the equatorial Atlantic (Figure 54) but also in the equatorial
570 Pacific (Figure ??). ~~Further investigations are needed to analyse the changes in SST variability in the equatorial Pacific and~~
their origins 10d). Due to its disproportionate role in the global climate at interannual and longer variabilities, further studies
should focus on assessing the equatorial Pacific as represented by OMIP1 and OMIP2 models.

Code availability.

The MOM numerical ocean model version 5 is available from <https://github.com/mom-ocean/MOM5>. The scripts to repro-
575 duce the figures of the manuscript are available upon request to the corresponding author.

Data availability.

The ORA-S5 data is publicly available at the link: [https://cds.climate.copernicus.eu/cdsapp#!/dataset/reanalysis-oras5?tab=](https://cds.climate.copernicus.eu/cdsapp#!/dataset/reanalysis-oras5?tab=form) form. The OI-SST data is publicly available at the link: <https://psl.noaa.gov/data/gridded/data.noaa.oisst.v2.html>. The CCMP v2 data is publicly available at the following link: https://apdrc.soest.hawaii.edu/erddap/griddap/hawaii_soest_3387_f2e3_e359.html. The AVISO SLA was retrieved at the following link: <https://cds.climate.copernicus.eu/cdsapp#!/dataset/10.24381/cds.4c328c78?tab=overview>. The ~~NCEP-R1 data is publicly available at the following link: . The NCEP/DOE-R2 data is publicly available at the following link: . The ERA5 data is available at the following link: .~~

~~The~~ OMIP1 and OMIP2 model output data were downloaded at the following link: <https://esgf-data.dkrz.de/projects/esgf-dkrz/>. The CORE-II forcing is available at the following link: <https://data1.gfdl.noaa.gov/nomads/forms/core/COREv2.html>. The JRA55-do forcing is available at the following link: <https://climate.mri-jma.go.jp/pub/ocean/JRA55-do/>. The MOM5-LR, ~~MOM5-LR-winds, MOM5-LR-heat~~ MOM5-LR-anom, and MOM5-HR datasets used in this study can be retrieved from ~~Farneti (2023)~~ Farneti (2024).

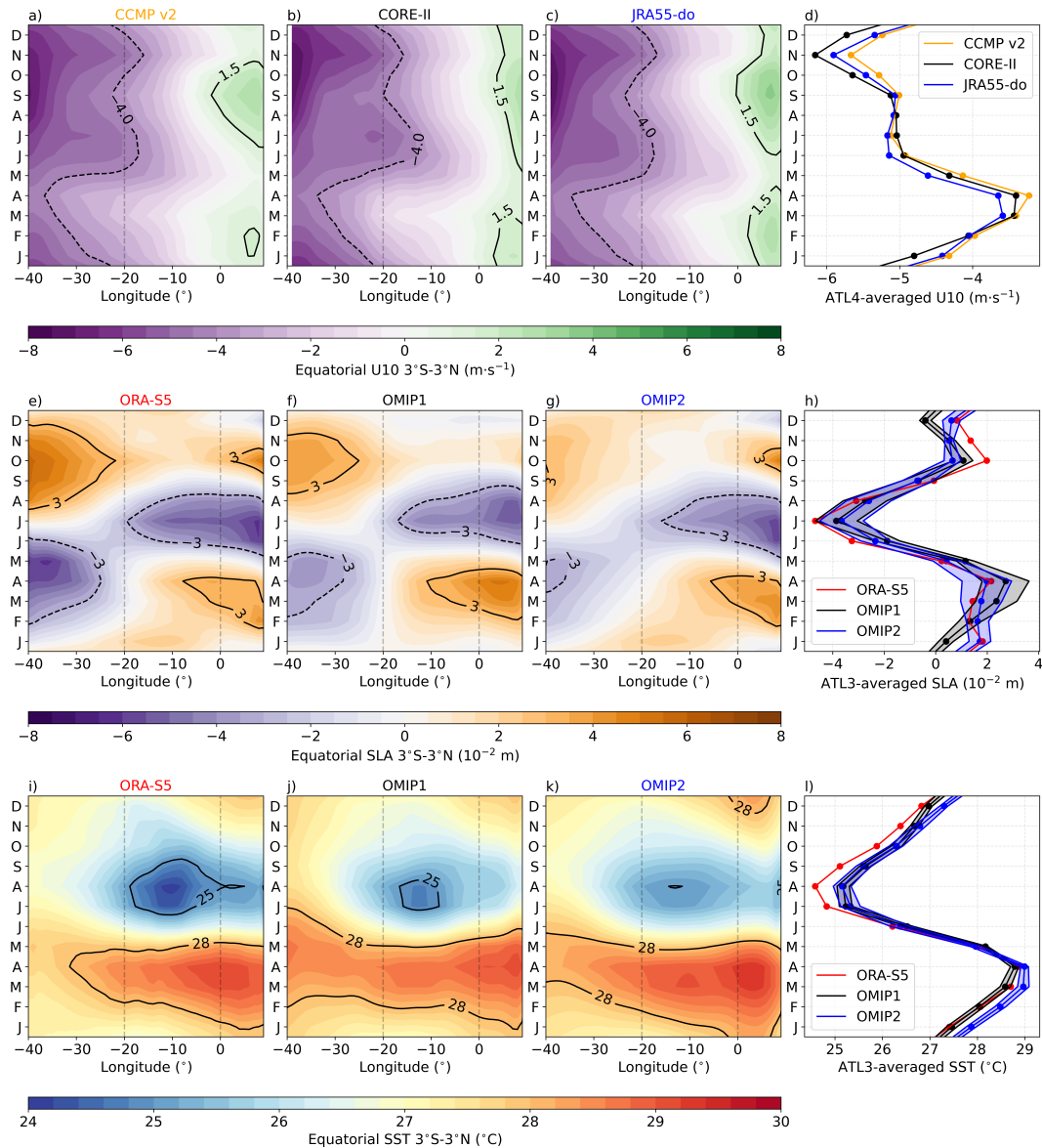


Figure 2. Hovmöller diagrams illustrating seasonal cycles in the monthly climatologies for equatorial Atlantic U10, SLA, and SST. (a) The seasonal cycle Monthly climatology of CCMP v2 U10, averaged between 3°S and 3°N and presented as a function of longitude and calendar month for the period January 1987 to December 2004. (b) The seasonal cycle of CORE-II zonal wind, averaged between 3°S and 3°N, displayed as a function of the longitude and calendar month for the period January 1985 to December 2004. (c) Same same as (b) but for the CORE-II and JRA55-do U10. (d) The seasonal cycle of SLA in ORA-S5, averaged between 3°S and 3°N, shown as a function of over the longitude and calendar month for the period from January 1985 to December 2004. (e) Similar to (d) but for Monthly climatologies of the OMIP1 ensemble mean. ATL4-averaged U10 from CCMP v2 (for orange) Same as CORE-II (d) (black) but for the OMIP2 ensemble mean, and JRA55-do (blue). (e, f, g) the seasonal cycle Monthly climatologies of SST SLA in ORA-S5, OMIP1 ensemble mean, and OMIP2 ensemble mean, averaged between 3°S and 3°N, presented shown as a function of the longitude and calendar month for the period from January 1985 to December 2004. (h) Similar to Monthly climatologies of the ATL3-averaged SLA from ORA-S5 (red) but representing the OMIP1 ensemble mean (black), and OMIP2 (blue). (i, j, k, l) Same as (e, f, g, h) but for the OMIP2 ensemble mean SST.

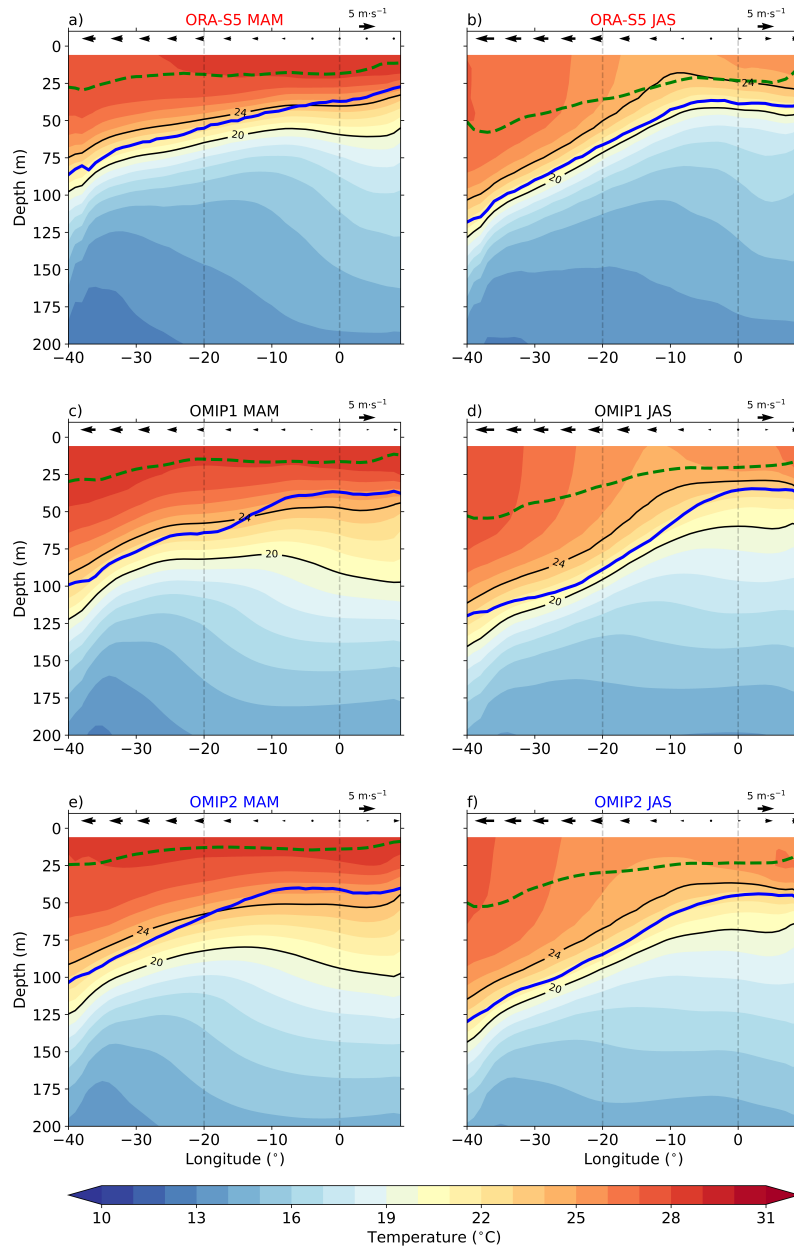


Figure 3. Upper 200 m ocean temperature for MAM (left) and JAS (right). (a, c, e) MAM upper 200 m ocean temperature in the equatorial Atlantic (40°W - 9°E , 3°S - 3°N) with shading, where black arrows indicate zonal wind at 10 m height, thick blue lines denote the maximum dT/dz , green dashed lines represent the mixed layer depth, and black lines indicate the depths of the 20°C and 25 - 24°C isotherms for ORA-S5, OMIP1 and OMIP2 ensemble means, respectively. (b, d, f) Same as (a, c, e) but for JAS. (d, h) Vertical ocean velocity profiles averaged over the ATL3 region in MAM for the OMIP1 and OMIP2 ensemble means, respectively. Shaded areas represent the ensembles' spreads, estimated as ± 1 standard deviation. (f, j) Same as (d, h) but for JAS. Vertical black dashed lines denote the ATL3 region.

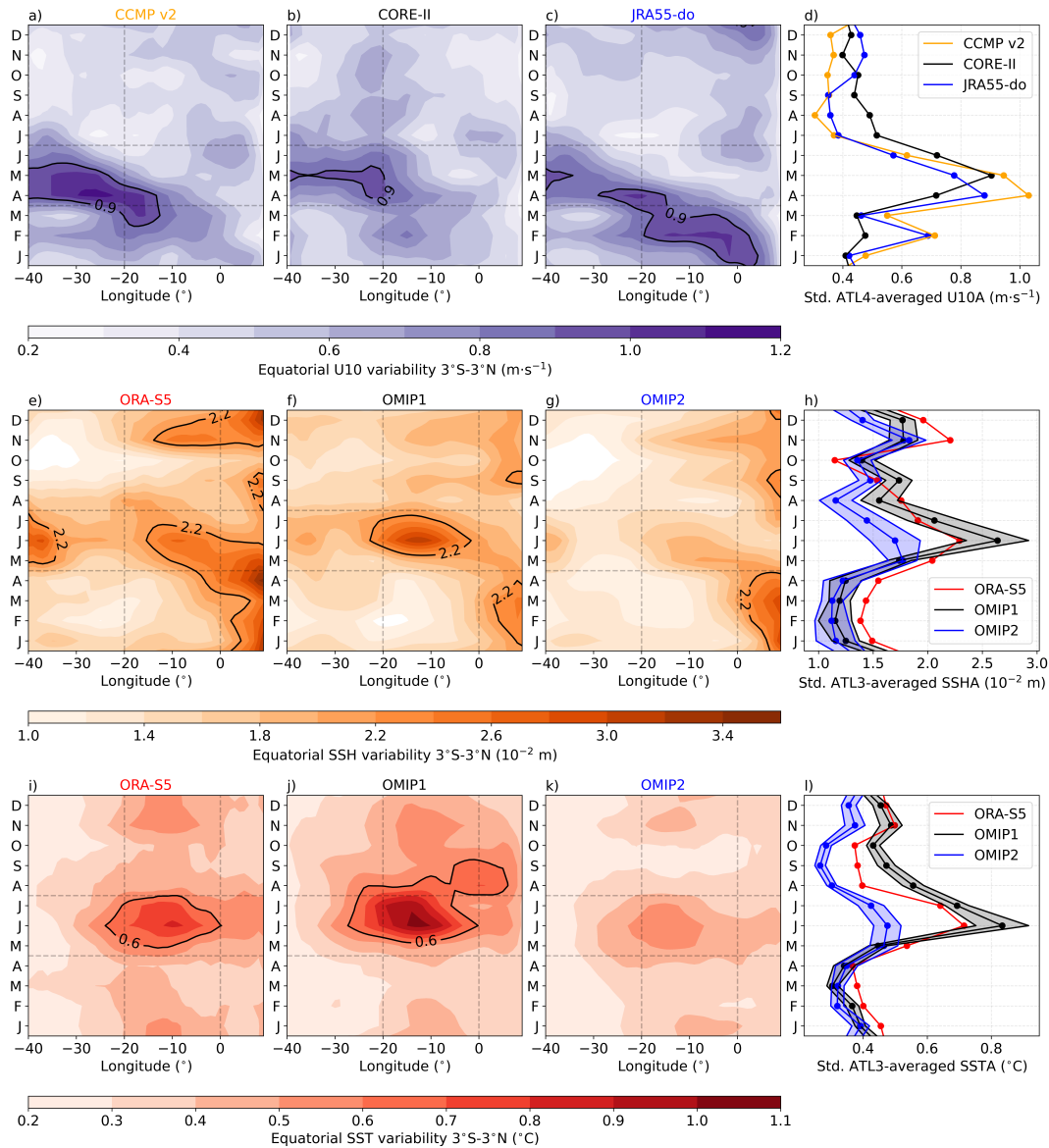


Figure 4. Hovmöller diagrams depicting equatorial Atlantic U10, SSH and SST interannual variability. (a) Standard deviation of CCMP v2 U10 anomalies averaged between 3°S and 3°N, plotted as a function of longitude and calendar month, spanning from January 1987 to December 2004. (b) Standard deviation of CORE-II zonal wind anomalies, averaged between 3°S and 3°N, and displayed as a function of longitude and calendar month for the period from January 1985 to December 2004. (c) Same as (b) but for JRA55-do U10. (d) Standard deviation of the monthly climatological standard deviation of SSH interannual anomalies, averaged between 3°S and 3°N, and plotted as a function of longitude and calendar month for the period January 1985 to December 2004. (e) Same as (d) but for the OMIP1 ensemble mean. (f, g, i, j, k) Same as (d) but for the OMIP2 ensemble mean. (h) Standard deviation of the monthly climatological standard deviation of SST interannual anomalies, averaged between 3°S and 3°N, plotted as a function of longitude and calendar month for the period from January 1985 to December 2004. (i) Same as (h) but for the OMIP1 ensemble mean. (j, k) Same as (h) but for the OMIP2 ensemble mean.

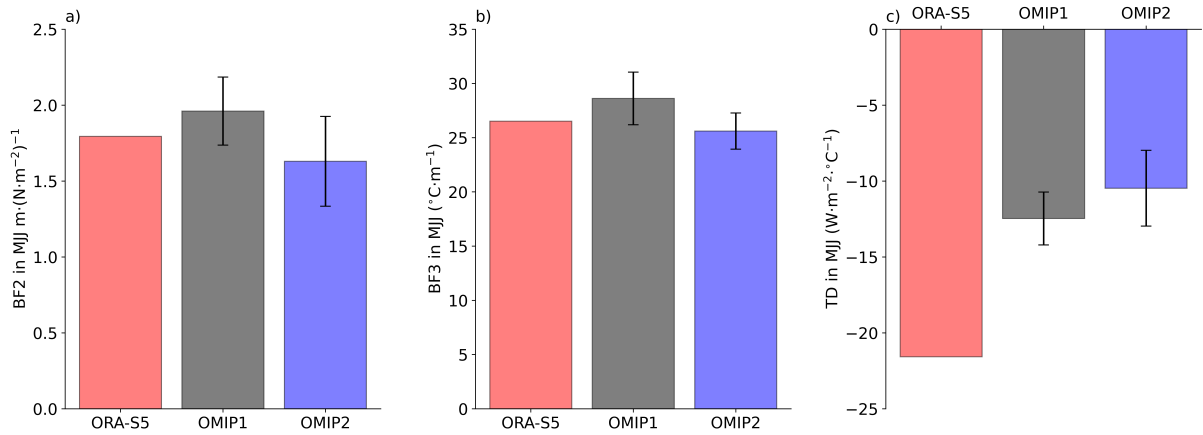


Figure 5. Bjerknes feedback components and thermal damping during MJJ over the period from January 1985 to December 2004. (a) Histogram of the ~~BF1~~BF2 in MJJ for ORA-S5 (grey), the OMIP1 ensemble (blue), and the OMIP2 ensemble (red). (b) Same as (a) but for the ~~BF2~~BF3. (c) Same as (a) but for the ~~BF3~~. (d) Same as (a) but for the thermal damping (TD). Error bars are defined as \pm one standard deviation of the ensemble.

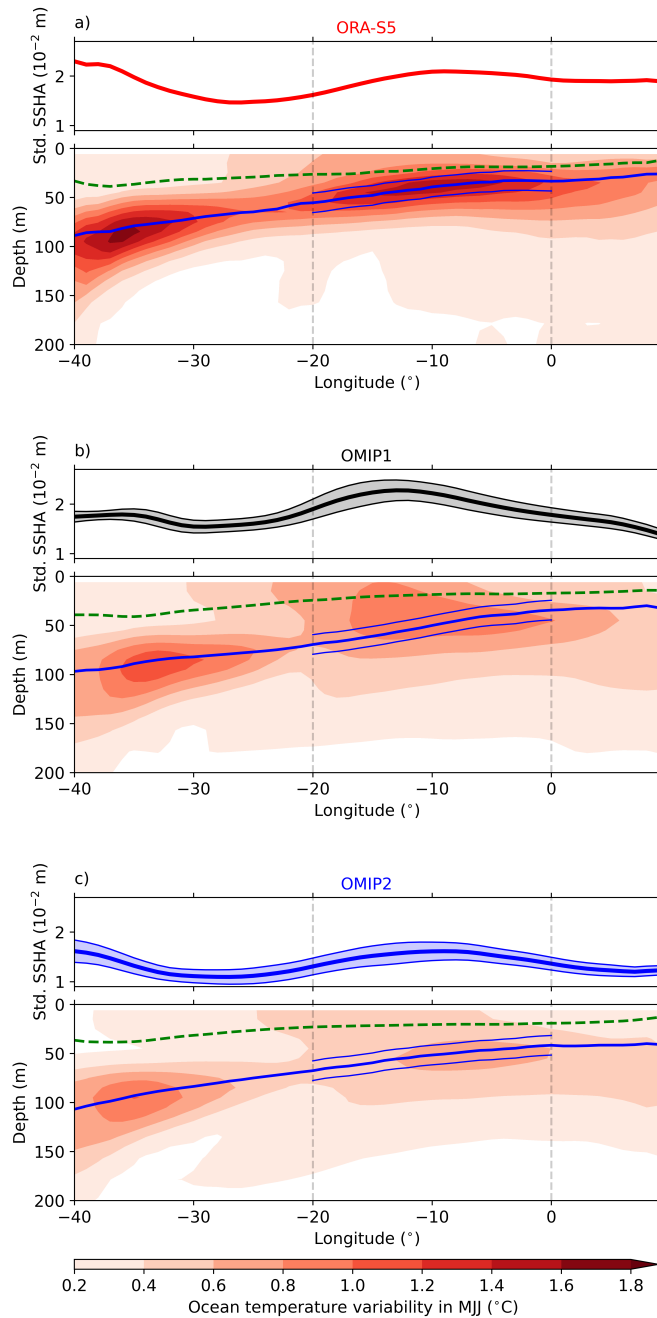


Figure 6. Interannual Equatorial Atlantic (40°W - 9°E , 3°S - 3°N) interannual variability of SSH and upper 200 m ocean temperature during MJJ over the period from January 1985 to December 2004. Upper 200 m ocean temperature interannual variability in the equatorial Atlantic (40°W - 9°E , 3°S - 3°N) 2004 for (a) ORA-S5, (b) the OMIP1 ensemble mean, and (c) the OMIP2 ensemble mean. Thick blue lines represent the depth of maximum dT/dz , while green dashed lines denote the mixed layer depth. Thin blue lines encompass a ± 10 m range around the mean thermocline. Vertical dashed lines in black denote the ATL3 region.

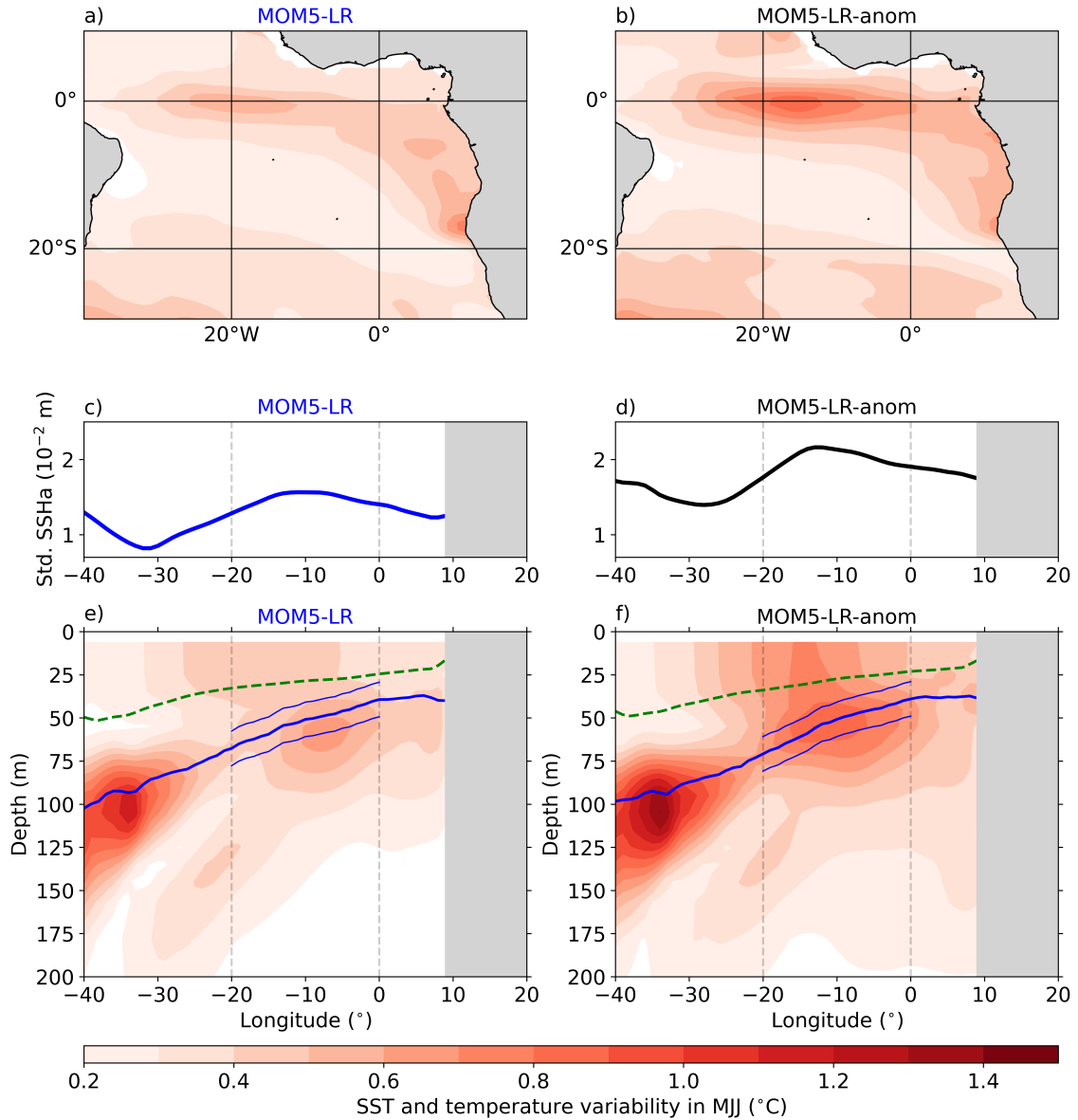


Figure 7. Interannual SST, SSH and upper 200 m temperature variability during MJJ over the period from January 1985 to December 2004. (a) Standard deviation of SST anomalies averaged over MJJ for (a)-MOM5-LR and (b) MOM5-LR-winds. Standard deviation of temperature-SSH anomalies within-in the upper-200-m depth-of-the equatorial Atlantic (3°S - 3°N) during MJJ for MOM5-LR. (ae) Standard deviation of the equatorial Atlantic MJJ upper 200 m temperature anomalies for MOM5-LR and (b, d, f) MOM5-LR-winds Same as (a, c, e) but for MOM5-LR-anom. The dashed green lines represent the MLD. The solid blue lines indicate the depth of the maximum vertical temperature gradient in MJJ. Thin blue lines encompass a ± 10 m range around the mean thermocline. Vertical dashed black lines denote the ATL3 region.

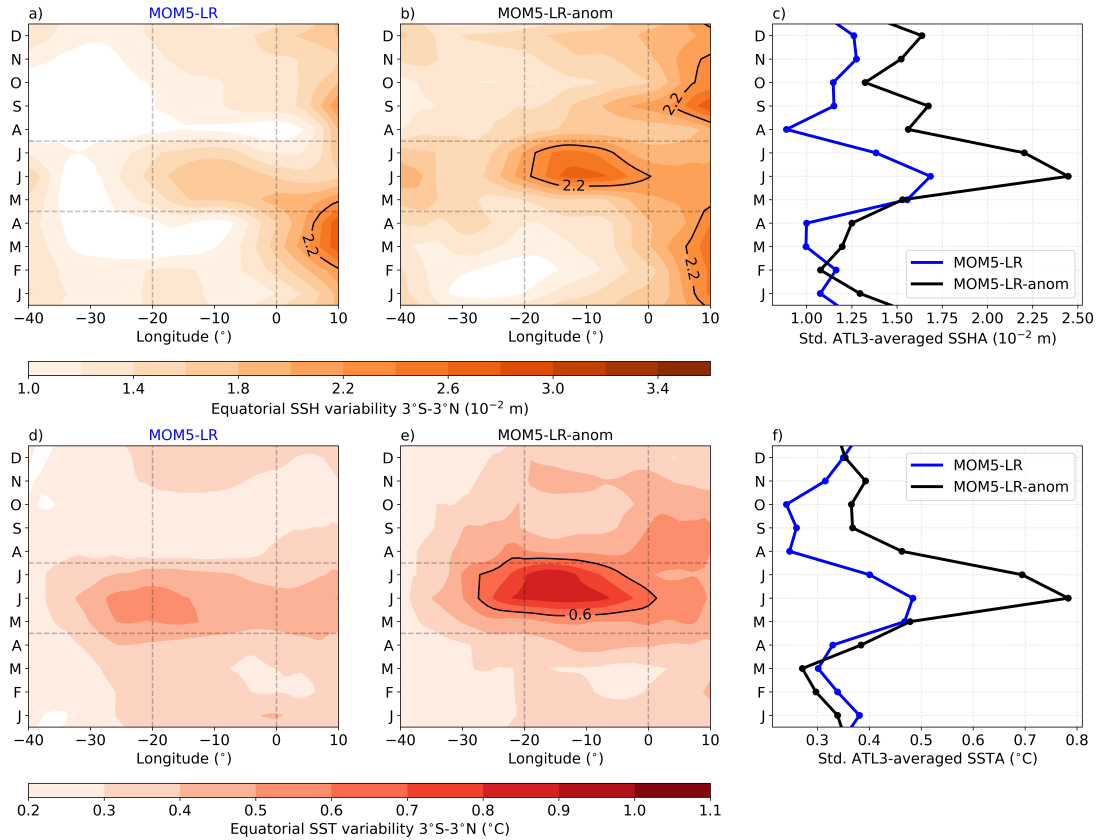


Figure 8. Hovmöller diagrams depicting the interannual variability of SSH and SST over the period from January 1985 to December 2004. (a) Standard Monthly climatological standard deviation of the MOM5-LR SSH anomalies SSHA, averaged between 3°S and 3°N, plotted as a function of longitude and calendar month. (b) Same as (a) but for MOM5-LR winds MOM5-LR-anom. (c) Standard Monthly climatological standard deviation of the ATL3-averaged SSHA for MOM5-LR SST anomalies, averaged between 3°S (blue) and 3°N, plotted as a function of longitude and calendar month MOM5-LR-anom (black). (d, e, f) Same as (a, b, c) but for MOM5-LR winds the SSTA.

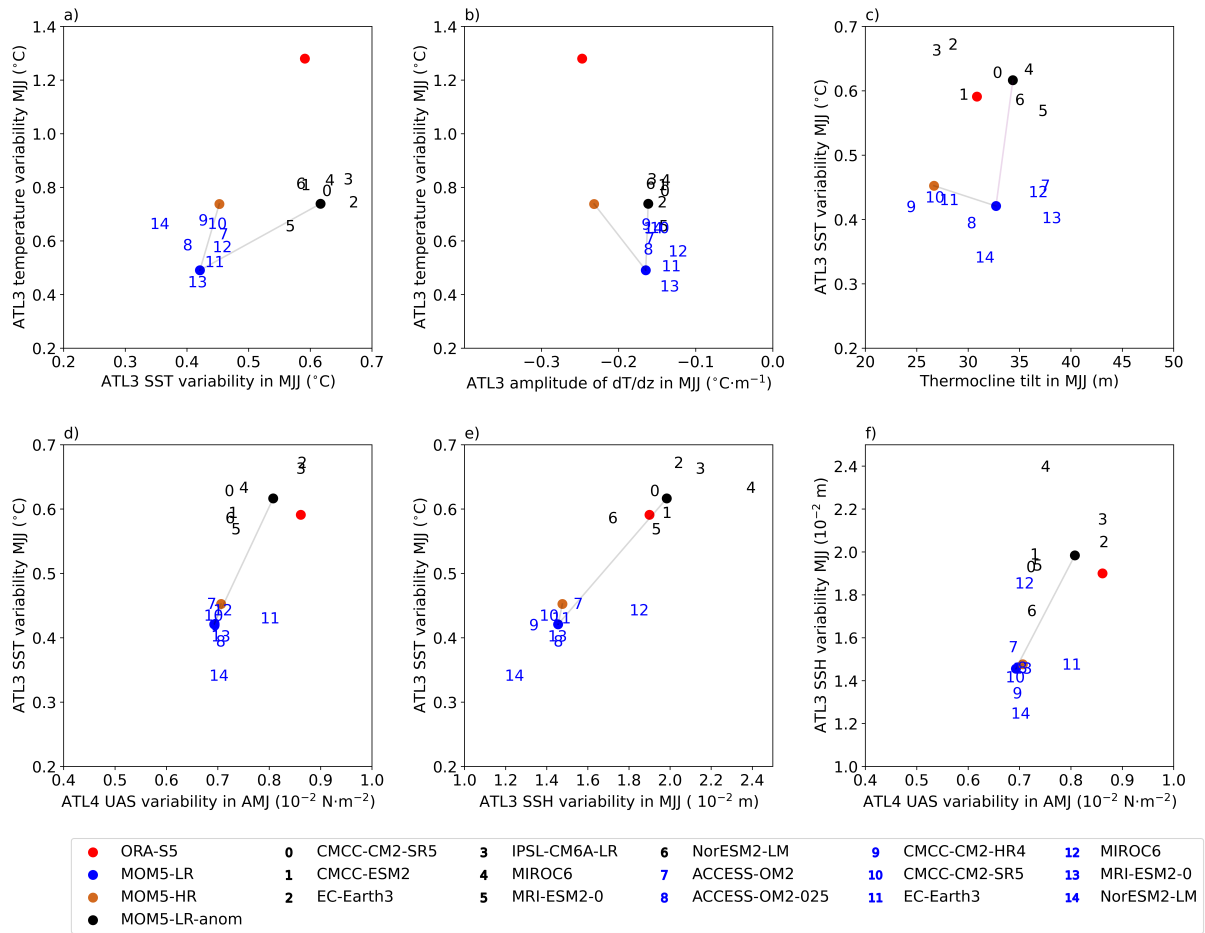


Figure 9. Scatter plots illustrating various equatorial Atlantic metrics assessed during the period January 1985 to December 2004. (a) Relationship between the standard deviation of ATL3-averaged SST anomalies in MJJ and the ATL3-averaged temperature anomalies in MJJ within ± 10 m around the mean thermocline. (b) Relationship between ATL3-averaged dT/dz within ± 10 m around the mean thermocline in MJJ and the ATL3-averaged temperature anomalies in MJJ within ± 10 m around the mean thermocline. (c) Relationship between the equatorial Atlantic thermocline tilt in MJJ and the standard deviation of ATL3-averaged SST anomalies in MJJ. The equatorial thermocline tilt is defined as the difference between ATL4-averaged and ATL3-averaged depth of the maximum dT/dz . (d) Relationship between the standard deviation of ATL4-averaged UAS anomalies in MJJ and the standard deviation of ATL3-averaged SST anomalies in MJJ. (e) Relationship between the standard deviation of ATL3-averaged SSH anomalies in MJJ and the standard deviation of ATL3-averaged SST anomalies in MJJ. (f) Relationship between the standard deviation of ATL4-averaged UAS anomalies in MJJ and the standard deviation of ATL3-averaged SSH anomalies in MJJ. Dots are colour-coded: black, red, green, blue, brown, purple, and cyan-black dots represent ORA-S5, MOM5-LR, MOM5-HR, MOM5-LR-winds, and MOM5-LR-heat, MOM5-LR-anom, respectively. Blue-Black (red-blue) numbers denote the OMIP1 (OMIP2) models.

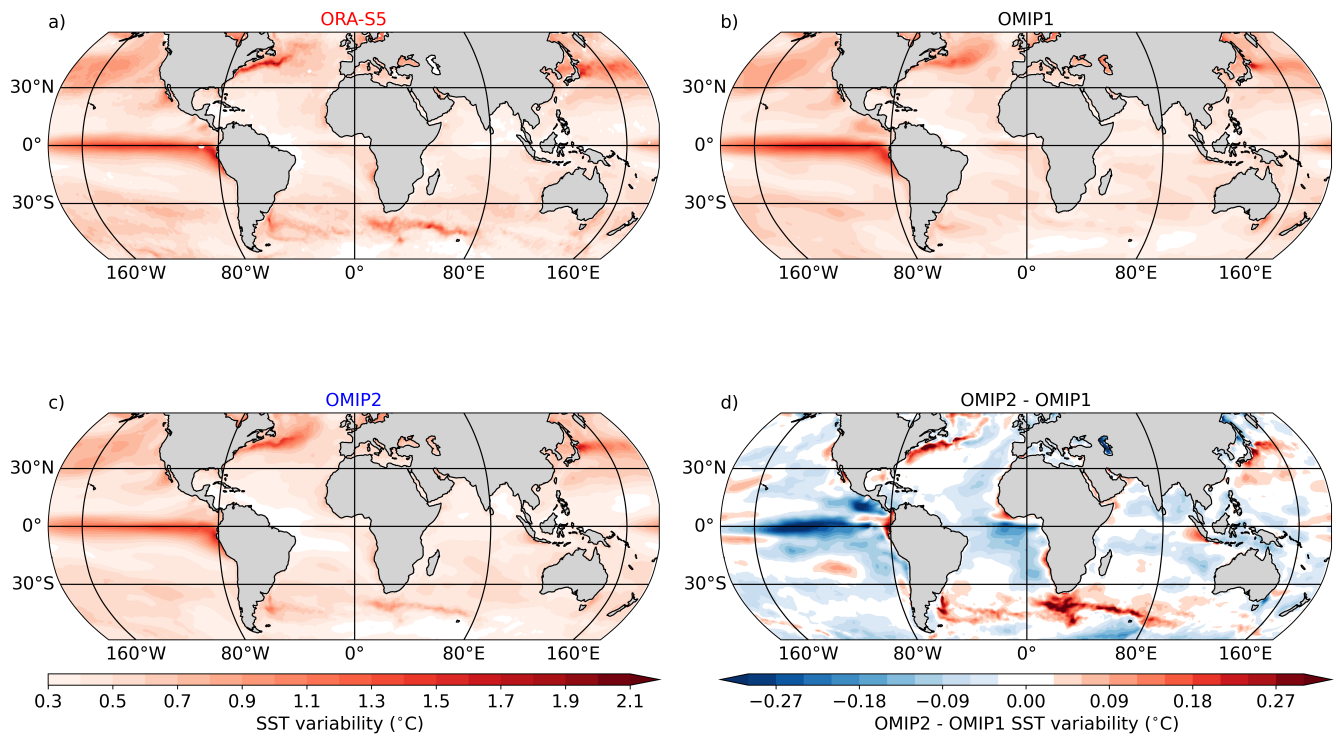


Figure 10. Standard deviation of monthly mean SST anomalies for (a) ORA-S5, (b) the OMIP1 ensemble mean, (c) the OMIP2 ensemble mean spanning from January 1985 to December 2004, (d) Difference between the OMIP2 ensemble mean minus the OMIP1 ensemble mean.

Author contributions.

AP carried out the analyses and wrote the first draft of the manuscript. RF ran the sensitivity experiments and participated
590 in the conceptualization, editing, and reviewing of the manuscript.

Competing interests.

The authors declare no competing interests.

Acknowledgements. We acknowledge the infrastructure and financial support of The Abdus Salam International Center for Theoretical
Physics (ICTP). We also thank the climate modelling groups for producing and making available their model output, the Earth System Grid
595 Federation (ESGF) for archiving the data and providing access.

References

- Adcroft, A., Anderson, W., Balaji, V., Blanton, C., Bushuk, M., Dufour, C. O., Dunne, J. P., Griffies, S. M., Hallberg, R., Harrison, M. J., Held, I. M., Jansen, M. F., John, J. G., Krasting, J. P., Langenhorst, A. R., Legg, S., Liang, Z., McHugh, C., Radhakrishnan, A., Reichl, B. G., Rosati, T., Samuels, B. L., Shao, A., Stouffer, R., Winton, M., Wittenberg, A. T., Xiang, B., Zadeh, N., and Zhang, R.: The GFDL
600 Global Ocean and Sea Ice Model OM4.0: Model Description and Simulation Features, *Journal of Advances in Modeling Earth Systems*, 11, 3167–3211, <https://doi.org/https://doi.org/10.1029/2019MS001726>, 2019.
- Bjerknes, J.: ATMOSPHERIC TELECONNECTIONS FROM THE EQUATORIAL PACIFIC, *Monthly Weather Review*, 97, 163 – 172, [https://doi.org/https://doi.org/10.1175/1520-0493\(1969\)097<0163:ATFTEP>2.3.CO;2](https://doi.org/https://doi.org/10.1175/1520-0493(1969)097<0163:ATFTEP>2.3.CO;2), 1969.
- Bleck, R.: An oceanic general circulation model framed in hybrid isopycnic-Cartesian coordinates, *Ocean Modelling*, 4, 55–88,
605 [https://doi.org/https://doi.org/10.1016/S1463-5003\(01\)00012-9](https://doi.org/https://doi.org/10.1016/S1463-5003(01)00012-9), 2002.
- Bourlès, B., Lumpkin, R., McPhaden, M. J., Hernandez, F., Nobre, P., Campos, E., Yu, L., Planton, S., Busalacchi, A., Moura, A. D., Servain, J., and Trotte, J.: THE PIRATA PROGRAM: History, Accomplishments, and Future Directions*, *Bulletin of the American Meteorological Society*, 89, 1111 – 1126, <https://doi.org/10.1175/2008BAMS2462.1>, 2008.
- Brandt, P., Caniaux, G., Bourlès, B., Lazar, A., Dengler, M., Funk, A., Hormann, V., Giordani, H., and Marin, F.: Equato-
610 rial upper-ocean dynamics and their interaction with the West African monsoon, *Atmospheric Science Letters*, 12, 24–30, <https://doi.org/https://doi.org/10.1002/asl.287>, 2011.
- Brandt, P., Claus, M., Greatbatch, R. J., Kopte, R., Toole, J. M., Johns, W. E., and Böning, C. W.: Annual and Semiannual Cycle of Equatorial Atlantic Circulation Associated with Basin-Mode Resonance, *Journal of Physical Oceanography*, 46, 3011 – 3029, <https://doi.org/10.1175/JPO-D-15-0248.1>, 2016.
- 615 Burls, N. J., Reason, C. J. C., Penven, P., and Philander, S. G.: Energetics of the Tropical Atlantic Zonal Mode, *Journal of Climate*, 25, 7442 – 7466, <https://doi.org/10.1175/JCLI-D-11-00602.1>, 2012.
- Caniaux, G., Giordani, H., Redelsperger, J.-L., Guichard, F., Key, E., and Wade, M.: Coupling between the Atlantic cold tongue and the West African monsoon in boreal spring and summer, *Journal of Geophysical Research: Oceans*, 116, <https://doi.org/https://doi.org/10.1029/2010JC006570>, 2011.
- 620 Cassou, C., Terray, L., and Phillips, A. S.: Tropical Atlantic Influence on European Heat Waves, *Journal of Climate*, 18, 2805 – 2811, <https://doi.org/10.1175/JCLI3506.1>, 2005.
- Chenillat, F., Illig, S., Jouanno, J., Awo, F. M., Alory, G., and Brehmer, P.: How do Climate Modes Shape the Chlorophyll-a Interannual Variability in the Tropical Atlantic?, *Geophysical Research Letters*, 48, e2021GL093769, <https://doi.org/https://doi.org/10.1029/2021GL093769>, e2021GL093769 2021GL093769, 2021.
- 625 Crespo, L. R., Prigent, A., Keenlyside, N., Koseki, S., Svendsen, L., Richter, I., and Sánchez-Gómez, E.: Weakening of the Atlantic Niño variability under global warming, *Nature Climate Change*, 12, 822–827, <https://doi.org/10.1038/s41558-022-01453-y>, 2022.
- Davey, M., Huddleston, M., Sperber, K., Braconnot, P., Bryan, F., Chen, D., Colman, R., Cooper, C., Cubasch, U., Delecluse, P., DeWitt, D., Fairhead, L., Flato, G., Gordon, C., Hogan, T., Ji, M., Kimoto, M., Kitoh, A., Knutson, T., Latif, M., Le Treut, H., Li, T., Manabe, S., Mechoso, C., Meehl, G., Power, S., Roeckner, E., Terray, L., Vintzileos, A., Voss, R., Wang, B., Washington, W., Yoshikawa, I., Yu, J.,
630 Yukimoto, S., and Zebiak, S.: STOIC: a study of coupled model climatology and variability in tropical ocean regions, *Climate Dynamics*, 18, 403–420, <https://doi.org/10.1007/s00382-001-0188-6>, 2002.

- Deppenmeier, A.-L., Haarsma, R. J., and Hazeleger, W.: The Bjerknes feedback in the tropical Atlantic in CMIP5 models, *Climate Dynamics*, 47, 2691–2707, <https://doi.org/10.1007/s00382-016-2992-z>, 2016.
- Deser, C., Alexander, M. A., Xie, S.-P., and Phillips, A. S.: Sea Surface Temperature Variability: Patterns and Mechanisms, *Annual Review of Marine Science*, 2, 115–143, <https://doi.org/10.1146/annurev-marine-120408-151453>, 2009.
- Ding, H., Keenlyside, N. S., and Latif, M.: Seasonal cycle in the upper equatorial Atlantic Ocean, *Journal of Geophysical Research: Oceans*, 114, <https://doi.org/https://doi.org/10.1029/2009JC005418>, 2009.
- Dippe, T., Lübbecke, J. F., and Greatbatch, R. J.: A Comparison of the Atlantic and Pacific Bjerknes Feedbacks: Seasonality, Symmetry, and Stationarity, *Journal of Geophysical Research: Oceans*, 124, 2374–2403, <https://doi.org/https://doi.org/10.1029/2018JC014700>, 2019.
- 640 Farneti, R.: Output files for MOM5 driven by JRA55-do at 1-degree and 0.25-degree horizontal resolution, <https://doi.org/10.5281/zenodo.10219517>, 2023.
- Farneti, R.: Output files for MOM5 driven by JRA55-do at 1-degree and 0.25-degree horizontal resolution, <https://doi.org/10.5281/zenodo.11047949>, 2024.
- Farneti, R., Stiz, A., and Ssebandeke, J. B.: Improvements and persistent biases in the southeast tropical Atlantic in CMIP models, *npj Climate and Atmospheric Science*, 5, 42, <https://doi.org/10.1038/s41612-022-00264-4>, 2022.
- Folland, C. K., Palmer, T. N., and Parker, D. E.: Sahel rainfall and worldwide sea temperatures, 1901–85, *Nature*, 320, 602–607, <https://doi.org/10.1038/320602a0>, 1986.
- Fox-Kemper, B., Ferrari, R., and Hallberg, R.: Parameterization of Mixed Layer Eddies. Part I: Theory and Diagnosis, *Journal of Physical Oceanography*, 38, 1145 – 1165, <https://doi.org/https://doi.org/10.1175/2007JPO3792.1>, 2008.
- 650 Fox-Kemper, B., Danabasoglu, G., Ferrari, R., Griffies, S., Hallberg, R., Holland, M., Maltrud, M., Peacock, S., and Samuels, B.: Parameterization of mixed layer eddies. III: Implementation and impact in global ocean climate simulations, *Ocean Modelling*, 39, 61–78, <https://doi.org/https://doi.org/10.1016/j.ocemod.2010.09.002>, modelling and Understanding the Ocean Mesoscale and Submesoscale, 2011.
- Gent, P. R. and McWilliams, J. C.: Isopycnal Mixing in Ocean Circulation Models, *Journal of Physical Oceanography*, 20, 150 – 155, [https://doi.org/https://doi.org/10.1175/1520-0485\(1990\)020<0150:IMIOCM>2.0.CO;2](https://doi.org/https://doi.org/10.1175/1520-0485(1990)020<0150:IMIOCM>2.0.CO;2), 1990.
- Gent, P. R., Willebrand, J., McDougall, T. J., and McWilliams, J. C.: Parameterizing Eddy-Induced Tracer Transports in Ocean Circulation Models, *Journal of Physical Oceanography*, 25, 463 – 474, [https://doi.org/https://doi.org/10.1175/1520-0485\(1995\)025<0463:PEITTI>2.0.CO;2](https://doi.org/https://doi.org/10.1175/1520-0485(1995)025<0463:PEITTI>2.0.CO;2), 1995.
- Griffies, S.: Elements of MOM4p1, GFDL Ocean Group Tech. Rep. 6, 6, 2009.
- 660 Griffies, S. M.: The Gent–McWilliams Skew Flux, *Journal of Physical Oceanography*, 28, 831 – 841, [https://doi.org/https://doi.org/10.1175/1520-0485\(1998\)028<0831:TGMSF>2.0.CO;2](https://doi.org/https://doi.org/10.1175/1520-0485(1998)028<0831:TGMSF>2.0.CO;2), 1998.
- Griffies, S. M.: Elements of the Modular Ocean Model (MOM) (2012 Release), GFDL Ocean Group Technical Report No.7, NOAA/Geophysical Fluid Dynamics Laboratory, 618 + xiii pages, 2012.
- Griffies, S. M., Biastoch, A., Böning, C., Bryan, F., Danabasoglu, G., Chassignet, E. P., England, M. H., Gerdes, R., Haak, H., Hallberg, R. W., Hazeleger, W., Jungclaus, J., Large, W. G., Madec, G., Pirani, A., Samuels, B. L., Scheinert, M., Gupta, A. S., Severijns, C. A., Simmons, H. L., Treguier, A. M., Winton, M., Yeager, S., and Yin, J.: Coordinated Ocean-ice Reference Experiments (COREs), *Ocean Modelling*, 26, 1–46, <https://doi.org/https://doi.org/10.1016/j.ocemod.2008.08.007>, 2009.
- Griffies, S. M., Danabasoglu, G., Durack, P. J., Adcroft, A. J., Balaji, V., Böning, C. W., Chassignet, E. P., Curchitser, E., Deshayes, J., Drange, H., Fox-Kemper, B., Gleckler, P. J., Gregory, J. M., Haak, H., Hallberg, R. W., Heimbach, P., Hewitt, H. T., Holland, D. M.,

- 670 Ilyina, T., Jungclaus, J. H., Komuro, Y., Krasting, J. P., Large, W. G., Marsland, S. J., Masina, S., McDougall, T. J., Nurser, A. J. G., Orr, J. C., Pirani, A., Qiao, F., Stouffer, R. J., Taylor, K. E., Treguier, A. M., Tsujino, H., Uotila, P., Valdivieso, M., Wang, Q., Winton, M., and Yeager, S. G.: OMIP contribution to CMIP6: experimental and diagnostic protocol for the physical component of the Ocean Model Intercomparison Project, *Geoscientific Model Development*, 9, 3231–3296, <https://doi.org/10.5194/gmd-9-3231-2016>, 2016.
- Griffies, S. M., Adcroft, A., and Hallberg, R. W.: A Primer on the Vertical Lagrangian-Remap Method in Ocean Models Based
675 on Finite Volume Generalized Vertical Coordinates, *Journal of Advances in Modeling Earth Systems*, 12, e2019MS001954, <https://doi.org/https://doi.org/10.1029/2019MS001954>, e2019MS001954 10.1029/2019MS001954, 2020.
- Hersbach, H., Bell, B., Berrisford, P., Biavati, G., Horányi, A., Muñoz Sabater, J., Nicolas, J., Peubey, C., Radu, R., Rozum, I., Schepers, D., Simmons, A., Soci, C., Dee, D., and Thépaut, J.-N.: ERA5 monthly averaged data on single levels from 1940 to present, Copernicus Climate Change Service (C3S) Climate Data Store (CDS), 2023.
- 680 Hirst, A. C. and Hastenrath, S.: Atmosphere-Ocean Mechanisms of Climate Anomalies in the Angola-Tropical Atlantic Sector, *Journal of Physical Oceanography*, 13, 1146 – 1157, [https://doi.org/https://doi.org/10.1175/1520-0485\(1983\)013<1146:AOMOCA>2.0.CO;2](https://doi.org/https://doi.org/10.1175/1520-0485(1983)013<1146:AOMOCA>2.0.CO;2), 1983.
- Illig, S., Dewitte, B., Ayoub, N., du Penhoat, Y., Reverdin, G., De Mey, P., Bonjean, F., and Lagerloef, G. S. E.: Interannual long equatorial waves in the tropical Atlantic from a high-resolution ocean general circulation model experiment in 1981–2000, *Journal of Geophysical Research: Oceans*, 109, <https://doi.org/https://doi.org/10.1029/2003JC001771>, 2004.
- 685 Imbol Koungue, R. A., Illig, S., and Rouault, M.: Role of interannual Kelvin wave propagations in the equatorial Atlantic on the Angola Benguela Current system, *Journal of Geophysical Research: Oceans*, 122, 4685–4703, <https://doi.org/https://doi.org/10.1002/2016JC012463>, 2017.
- Jouanno, J., Hernandez, O., and Sanchez-Gomez, E.: Equatorial Atlantic interannual variability and its relation to dynamic and thermodynamic processes, *Earth System Dynamics*, 8, 1061–1069, <https://doi.org/10.5194/esd-8-1061-2017>, 2017.
- 690 Kalnay, E., Kanamitsu, M., Kistler, R., Collins, W., Deaven, D., Gandin, L., Iredell, M., Saha, S., White, G., Woollen, J., Zhu, Y., Chelliah, M., Ebisuzaki, W., Higgins, W., Janowiak, J., Mo, K. C., Ropelewski, C., Wang, J., Leetmaa, A., Reynolds, R., Jenne, R., and Joseph, D.: The NCEP/NCAR 40-Year Reanalysis Project, *Bulletin of the American Meteorological Society*, 77, 437 – 472, [https://doi.org/https://doi.org/10.1175/1520-0477\(1996\)077<0437:TNYRP>2.0.CO;2](https://doi.org/https://doi.org/10.1175/1520-0477(1996)077<0437:TNYRP>2.0.CO;2), 1996.
- Kanamitsu, M., Ebisuzaki, W., Woollen, J., Yang, S.-K., Hnilo, J. J., Fiorino, M., and Potter, G. L.: NCEP–DOE AMIP-II Reanalysis (R-2),
695 *Bulletin of the American Meteorological Society*, 83, 1631 – 1644, <https://doi.org/https://doi.org/10.1175/BAMS-83-11-1631>, 2002.
- Keenlyside, N. S. and Latif, M.: Understanding Equatorial Atlantic Interannual Variability, *Journal of Climate*, 20, 131 – 142, <https://doi.org/https://doi.org/10.1175/JCLI3992.1>, 2007.
- Kucharski, F., Bracco, A., Yoo, J. H., and Molteni, F.: Atlantic forced component of the Indian monsoon interannual variability, *Geophysical Research Letters*, 35, <https://doi.org/https://doi.org/10.1029/2007GL033037>, 2008.
- 700 Large, W. G. and Yeager, S. G.: The global climatology of an interannually varying air–sea flux data set, *Climate Dynamics*, 33, 341–364, <https://doi.org/10.1007/s00382-008-0441-3>, 2009.
- Large, W. G., McWilliams, J. C., and Doney, S. C.: Oceanic vertical mixing: A review and a model with a nonlocal boundary layer parameterization, *Reviews of Geophysics*, 32, 363–403, <https://doi.org/https://doi.org/10.1029/94RG01872>, 1994.
- Lübbecke, J. F. and McPhaden, M. J.: Symmetry of the Atlantic Niño mode, *Geophysical Research Letters*, 44, 965–973,
705 <https://doi.org/https://doi.org/10.1002/2016GL071829>, 2017.

- Lübbecke, J. F., Rodríguez-Fonseca, B., Richter, I., Martín-Rey, M., Losada, T., Polo, I., and Keenlyside, N. S.: Equatorial Atlantic variability—Modes, mechanisms, and global teleconnections, *WIREs Climate Change*, 9, e527, <https://doi.org/https://doi.org/10.1002/wcc.527>, 2018.
- 710 Mears, C. A., Scott, J., Wentz, F. J., Ricciardulli, L., Leidner, S. M., Hoffman, R., and Atlas, R.: A Near-Real-Time Version of the Cross-Calibrated Multiplatform (CCMP) Ocean Surface Wind Velocity Data Set, *Journal of Geophysical Research: Oceans*, 124, 6997–7010, <https://doi.org/https://doi.org/10.1029/2019JC015367>, 2019.
- Nobre, P. and Shukla, J.: Variations of Sea Surface Temperature, Wind Stress, and Rainfall over the Tropical Atlantic and South America, *Journal of Climate*, 9, 2464 – 2479, [https://doi.org/https://doi.org/10.1175/1520-0442\(1996\)009<2464:VOSSTW>2.0.CO;2](https://doi.org/https://doi.org/10.1175/1520-0442(1996)009<2464:VOSSTW>2.0.CO;2), 1996.
- Okumura, Y. and Xie, S.-P.: Some Overlooked Features of Tropical Atlantic Climate Leading to a New Niño-Like Phenomenon, *Journal of*
715 *Climate*, 19, 5859 – 5874, <https://doi.org/10.1175/JCLI3928.1>, 2006.
- Philander, S. G. H. and Pacanowski, R. C.: A model of the seasonal cycle in the tropical Atlantic Ocean, *Journal of Geophysical Research: Oceans*, 91, 14 192–14 206, <https://doi.org/https://doi.org/10.1029/JC091iC12p14192>, 1986.
- Prigent, A., Imbol Koungue, R. A., Imbol Nkwinkwa, A. S. N., Beobide-Arsuaga, G., and Farneti, R.: Uncertainty on Atlantic Niño Variability Projections, *Geophysical Research Letters*, 50, e2023GL105 000, <https://doi.org/https://doi.org/10.1029/2023GL105000>, 2023a.
- 720 Prigent, A., Imbol Koungue, R. A., Lübbecke, J. F., Brandt, P., Harlaß, J., and Latif, M.: Future weakening of southeastern tropical Atlantic Ocean interannual sea surface temperature variability in a global climate model, *Climate Dynamics*, <https://doi.org/10.1007/s00382-023-07007-y>, 2023b.
- Prodhomme, C., Voldoire, A., Exarchou, E., Deppenmeier, A.-L., García-Serrano, J., and Guemas, V.: How Does the Seasonal Cycle Control Equatorial Atlantic Interannual Variability?, *Geophysical Research Letters*, 46, 916–922,
725 <https://doi.org/https://doi.org/10.1029/2018GL080837>, 2019.
- Reynolds, R. W., Rayner, N. A., Smith, T. M., Stokes, D. C., and Wang, W.: An Improved In Situ and Satellite SST Analysis for Climate, *Journal of Climate*, 15, 1609 – 1625, [https://doi.org/https://doi.org/10.1175/1520-0442\(2002\)015<1609:AIISAS>2.0.CO;2](https://doi.org/https://doi.org/10.1175/1520-0442(2002)015<1609:AIISAS>2.0.CO;2), 2002.
- Richter, I. and Tokinaga, H.: An overview of the performance of CMIP6 models in the tropical Atlantic: mean state, variability, and remote impacts, *Climate Dynamics*, 55, 2579–2601, <https://doi.org/10.1007/s00382-020-05409-w>, 2020.
- 730 Richter, I., Xie, S.-P., Wittenberg, A. T., and Masumoto, Y.: Tropical Atlantic biases and their relation to surface wind stress and terrestrial precipitation, *Climate Dynamics*, 38, 985–1001, <https://doi.org/10.1007/s00382-011-1038-9>, 2012.
- Rodríguez-Fonseca, B., Polo, I., García-Serrano, J., Losada, T., Mohino, E., Mechoso, C. R., and Kucharski, F.: Are Atlantic Niños enhancing Pacific ENSO events in recent decades?, *Geophysical Research Letters*, 36, <https://doi.org/https://doi.org/10.1029/2009GL040048>, 2009.
- 735 Saha, S., Moorthi, S., Pan, H.-L., Wu, X., Wang, J., Nadiga, S., Tripp, P., Kistler, R., Woollen, J., Behringer, D., Liu, H., Stokes, D., Grumbine, R., Gayno, G., Wang, J., Hou, Y.-T., ya Chuang, H., Juang, H.-M. H., Sela, J., Iredell, M., Treadon, R., Kleist, D., Delst, P. V., Keyser, D., Derber, J., Ek, M., Meng, J., Wei, H., Yang, R., Lord, S., van den Dool, H., Kumar, A., Wang, W., Long, C., Chelliah, M., Xue, Y., Huang, B., Schemm, J.-K., Ebisuzaki, W., Lin, R., Xie, P., Chen, M., Zhou, S., Higgins, W., Zou, C.-Z., Liu, Q., Chen, Y., Han, Y., Cucurull, L., Reynolds, R. W., Rutledge, G., and Goldberg, M.: The NCEP Climate Forecast System Reanalysis, *Bulletin of the American Meteorological Society*, 91, 1015 – 1058, <https://doi.org/https://doi.org/10.1175/2010BAMS3001.1>, 2010.
- 740 Servain, J., Picaut, J., and Merle, J.: Evidence of Remote Forcing in the Equatorial Atlantic Ocean, *Journal of Physical Oceanography*, 12, 457 – 463, [https://doi.org/https://doi.org/10.1175/1520-0485\(1982\)012<0457:EORFIT>2.0.CO;2](https://doi.org/https://doi.org/10.1175/1520-0485(1982)012<0457:EORFIT>2.0.CO;2), 1982.

- Servain, J., Busalacchi, A. J., McPhaden, M. J., Moura, A. D., Reverdin, G., Vianna, M., and Zebiak, S. E.: A Pilot Research Moored Array in the Tropical Atlantic (PIRATA), *Bulletin of the American Meteorological Society*, 79, 2019 – 2032, [https://doi.org/10.1175/1520-0477\(1998\)079<2019:APRMAI>2.0.CO;2](https://doi.org/10.1175/1520-0477(1998)079<2019:APRMAI>2.0.CO;2), 1998.
- 745 Taboada, F. G., Stock, C. A., Griffies, S. M., Dunne, J., John, J. G., Small, R. J., and Tsujino, H.: Surface winds from atmospheric reanalysis lead to contrasting oceanic forcing and coastal upwelling patterns, *Ocean Modelling*, 133, 79–111, <https://doi.org/https://doi.org/10.1016/j.ocemod.2018.11.003>, 2019.
- Treguier, A. M., de Boyer Montégut, C., Bozec, A., Chassignet, E. P., Fox-Kemper, B., McC. Hogg, A., Iovino, D., Kiss, A. E., Le Sommer, J., Li, Y., Lin, P., Lique, C., Liu, H., Serazin, G., Sidorenko, D., Wang, Q., Xu, X., and Yeager, S.: The mixed-layer depth in the
750 Ocean Model Intercomparison Project (OMIP): impact of resolving mesoscale eddies, *Geoscientific Model Development*, 16, 3849–3872, <https://doi.org/10.5194/gmd-16-3849-2023>, 2023.
- Tsujino, H., Urakawa, S., Nakano, H., Small, R. J., Kim, W. M., Yeager, S. G., Danabasoglu, G., Suzuki, T., Bamber, J. L., Bentsen, M., Böning, C. W., Bozec, A., Chassignet, E. P., Curchitser, E., Boeira Dias, F., Durack, P. J., Griffies, S. M., Harada, Y., Ilicak, M., Josey, S. A., Kobayashi, C., Kobayashi, S., Komuro, Y., Large, W. G., Le Sommer, J., Marsland, S. J., Masina, S., Scheinert, M., Tomita, H.,
755 Valdivieso, M., and Yamazaki, D.: JRA-55 based surface dataset for driving ocean–sea-ice models (JRA55-do), *Ocean Modelling*, 130, 79–139, <https://doi.org/https://doi.org/10.1016/j.ocemod.2018.07.002>, 2018.
- Tsujino, H., Urakawa, L. S., Griffies, S. M., Danabasoglu, G., Adcroft, A. J., Amaral, A. E., Arsouze, T., Bentsen, M., Bernardello, R., Böning, C. W., Bozec, A., Chassignet, E. P., Danilov, S., Dussin, R., Exarchou, E., Fogli, P. G., Fox-Kemper, B., Guo, C., Ilicak, M., Iovino, D., Kim, W. M., Koldunov, N., Lapin, V., Li, Y., Lin, P., Lindsay, K., Liu, H., Long, M. C., Komuro, Y., Marsland, S. J., Masina, S., Nummelin, A., Rieck, J. K., Ruprich-Robert, Y., Scheinert, M., Sicardi, V., Sidorenko, D., Suzuki, T., Tatebe, H., Wang, Q., Yeager, S. G., and
760 Yu, Z.: Evaluation of global ocean–sea-ice model simulations based on the experimental protocols of the Ocean Model Intercomparison Project phase 2 (OMIP-2), *Geoscientific Model Development*, 13, 3643–3708, <https://doi.org/10.5194/gmd-13-3643-2020>, 2020.
- Wahl, S., Latif, M., Park, W., and Keenlyside, N.: On the Tropical Atlantic SST warm bias in the Kiel Climate Model, *Climate Dynamics*, 36, 891–906, <https://doi.org/10.1007/s00382-009-0690-9>, 2011.
- 765 Wen, C., Xue, Y., Kumar, A., Behringer, D., and Yu, L.: How do uncertainties in NCEP R2 and CFSR surface fluxes impact tropical ocean simulations?, *Climate Dynamics*, 49, 3327–3344, <https://doi.org/10.1007/s00382-016-3516-6>, 2017.
- Xie, S.-P. and Carton, J. A.: Tropical Atlantic Variability: Patterns, Mechanisms, and Impacts, pp. 121–142, American Geophysical Union (AGU), <https://doi.org/https://doi.org/10.1029/147GM07>, 2004.
- Zebiak, S. E.: Air–Sea Interaction in the Equatorial Atlantic Region, *Journal of Climate*, 6, 1567 – 1586,
770 [https://doi.org/https://doi.org/10.1175/1520-0442\(1993\)006<1567:AIITEA>2.0.CO;2](https://doi.org/https://doi.org/10.1175/1520-0442(1993)006<1567:AIITEA>2.0.CO;2), 1993.
- Zhang, Q., Zhu, Y., and Zhang, R.-H.: Subsurface Warm Biases in the Tropical Atlantic and Their Contributions to the Role of Wind Forcing and Ocean Vertical Mixing, *Journal of Climate*, 35, 2291–2303, <https://doi.org/https://doi.org/10.1175/JCLI-D-21-0779.1>, 2022.
- Zuo, H., Balmaseda, M. A., Tietsche, S., Mogensen, K., and Mayer, M.: The ECMWF operational ensemble reanalysis–analysis system for ocean and sea ice: a description of the system and assessment, *Ocean Science*, 15, 779–808, <https://doi.org/10.5194/os-15-779-2019>,
775 2019.